Multilinear analysis of Time-Resolved Laser-Induced Fluorescence Spectra of U(VI) containing natural water samples

Jakub Višňák, [1,5,6,a], *Robin* Steudtner[2], *Andrea* Kassahun[4] and *Nils* Hoth[3]

[1]*Dept. of Nuclear Chemistry, FNSPE, Czech Technical University, Břehová 7, 115 19 Prague 1, Czech Rep.*
[2]*Institut für Radiochemie, Forschungszentrum Rossendorf e.V., P.O. Box 510119, 01314 Dresden, Germany*
[3]*Univ. of Mining and Technology, Dept. of Mining and Special Construction Engineering, Zeunerstr. 1A, 09596 Freiberg, Germany.*
[4]*WISMUT GmbH, Jagdschänkenstr. 29, 09117 Chemnitz, Germany.*
[5]*Dept. of Chemical Physics and Optics, Faculty of Mathematics and Physics, Charles Univ., Ke Karlovu 3, 121 16 Prague 2, Czech Rep.*
[6]*J. Heyrovský Institute of Physical Chemistry, Dolejškova 2155/3, 182 23 Prague 8, Czech Rep.*

Abstract. Natural waters' uranium level monitoring is of great importance for health and environmental protection. One possible detection method is the Time-Resolved Laser-Induced Fluorescence Spectroscopy (TRLFS), which offers the possibility to distinguish different uranium species. The analytical identification of aqueous uranium species in natural water samples is of distinct importance since individual species differ significantly in sorption properties and mobility in the environment. Samples originate from former uranium mine sites and have been provided by Wismut GmbH, Germany. They have been characterized by total elemental concentrations and TRLFS spectra. Uranium in the samples is supposed to be in form of uranyl(VI) complexes mostly with carbonate (CO_3^{2-}) and bicarbonate (HCO_3^-) and to lesser extend with sulphate (SO_4^{2-}), arsenate (AsO_4^{3-}), hydroxo (OH^-), nitrate (NO_3^-) and other ligands. Presence of alkaline earth metal dications ($M = Ca^{2+}$, Mg^{2+}, Sr^{2+}) will cause most of uranyl to prefer ternary complex species, e.g. $M_n(UO_2)(CO_3)_3^{2n-4}$ ($n \in \{1; 2\}$). From species quenching the luminescence, Cl^- and Fe^{2+} should be mentioned. Measurement has been done under cryogenic conditions to increase the luminescence signal. Data analysis has been based on Singular Value Decomposition and monoexponential fit of corresponding loadings (for separate TRLFS spectra, the "Factor analysis of Time Series" (FATS) method) and Parallel Factor Analysis (PARAFAC, all data analysed simultaneously). From individual component spectra, excitation energies T_{00}, uranyl symmetric mode vibrational frequencies ω_{gs} and excitation driven U-Oyl bond elongation ΔR have been determined and compared with quasirelativistic (TD)DFT/B3LYP theoretical predictions to cross-check experimental data interpretation.

1 Motivation

This contribution presents a first step in a longer run of both experimental and theoretical chemical (quantum chemistry and molecular dynamics) studies of uranium speciation in natural water samples and subsequent studies of possible chemical/physical remediation meeting criteria for health and environment protection.

A preliminary analysis of six samples TRLFS [1-6] spectra (S1-S5,S9) by FATS method [7] and of seven samples (the previously mentioned and S10) together by PARAFAC [8-12] will be presented.

The speciation, i.e. the information on how is given total analytical concentration of uranium partitioned into different chemical forms (coexisting in the same sample in chemical equilibrium), is of environmental importance because different chemical species will have different physical, chemical and biological properties such as mobility, toxicity and will require different measures for remediation. For example, studied samples are aerobic (E_H range from 130-450 mV), in pH range 5.5-9.3 and are supposed (based on analysis presented further) to consist dominantly of the neutral ternary complex $Ca_2UO_2(CO_3)_3^0$, the two-fold negatively charged $CaUO_2(CO_3)_3^{2-}$, $MgUO_2(CO_3)_3^{2-}$ (and to a lesser extent $UO_2(CO_3)_2^{2-}$, $UO_2(SO_4)_2^{2-}$) and the highly negative charged $UO_2(CO_3)_3^{4-}$. One of the remediation possibilities for uranium contaminated waters refers to the interaction of the water with anion-exchange resins, but the stable and by concentration dominating $Ca_2UO_2(CO_3)_3^0$

[a] Corresponding author: jvisnak@gmail.com

complex poses a problem, due to its electrical neutrality (and chemical equilibration changed by resin might not be fast enough in given experimental setup). But not all physical-chemical properties should be reduced to electric charge only, of course.

2 Theoretical background

2.1 Uranyl compounds spectra and optimal spectroscopic parameter choice

The aqueous uranyl complex compound luminescence theoretical background is briefly discussed in [1]. To shortcut the basis of it into two sentences – the luminescence corresponds to (by a good working hypothesis)[a] a single electronic transition on frontier molecular orbitals of central uranyl group (chromophore), and is resolved by a symmetric stretching vibrational mode of UO_2^{2+} group. The ligands coordinated to uranyl group can be seen as merely changing the excitation energy T_{00} of the transition, the vibrational frequencies ω_{gs}, ω_{es} and ΔR parameter mentioned later in text.

For a practical reasons, it should be stressed that while standard literature information on luminescence spectra (of individual chemical species in aqueous samples) consists of mere three to six luminescence band positions in nm (given usually with 1 nm precision), this might be a bit unfortunate format.

The reason is that since uranyl compounds luminescence spectra are very similar to each other, there is a need for a very careful spectroscopic parameter set choice. It is easy to observe that band positions, however in to-energy-proportional unit (e.g. cm^{-1}), form by (two) parts linear function of their ordinary number (please see Fig. 1,2 and Fig. 5 in [1])[b]. That is, both cold- and hot-bands are equidistant in cm^{-1} scale. The respective slopes in linear dependence on ordinary peak number n,

$$\frac{1}{\lambda_{n,m}} = \nu_{n,m} = T_{00,m} - \omega_m n , \qquad (1)$$

or "peak maxima spread"s correspond to "effective[c] symmetric stretching mode vibration frequency of uranyl, UO_2^{2+} (central) group" for electronic ground (cold-bands, ω_{gs} [cm^{-1}]) and luminescence-active excited state (hot-bands, ω_{es} [cm^{-1}]). The most energetic (highest in cm^{-1}) cold-band, (0'→0), peak energy complete the three parameter set (T_{00} [cm^{-1}], ω_{gs}, ω_{es}) describing all peak positions (no matter if they are three as well, or up to seven). While the linearity (or equidistances) of peak cm^{-1} position is usually very strong (uranyl group anharmonicity $\omega_e x_e$ is below 15 cm^{-1} [19-23] as compared to ω_{gs} = 870 cm^{-1} [1,23-25] for pentaaqua complex in water under ambient conditions) it is still better to obtain T_{00} as an intercept in linear regression of peak cm^{-1} positions instead of just 0'→0 peak position only. But storing seven peak positions seems to be rather redundant.

On the other side, the luminescence spectra shouldn't be reduced to band position information only – the way the signal is partitioned between different peaks (i.e. ratio of peak heights / areas under the peaks) provides important independent information. And since all spectroscopic parameters of individual uranyl chemical species coexisting in the same aqueous sample usually differ by quantity on an edge of experimental uncertainty (or even below) every piece of non-redundant spectral information matters greatly. Peak ratios information can be characterized by a property with a direct quantum chemical meaning (and therefore accessible by theoretical modelling) – the „excitational elongation" ΔR[pm] = $|R_{es} - R_{gs}|$, meaning an absolute value of difference between U-Oyl equilibrium bond length in electronic excited state (R_{es}) and in electronic ground state (R_{gs}, for further information, please see [1], the one-parameter fit with linear harmonic oscillator Franck-Condon factors for pentaaqua uranyl is given in Fig. 6 [1]).

Another independent information might be provided by individual peak FWHMs and their shapes (possible asymmetry or deviation from gaussian/voigt shape), but since this information is much more measurement-setup-dependent (e.g. the aperture slit widening will cause peak widening) and much less easy to interpret, it makes less sense to collect it.

For consistency check it is also important that certain independent spectroscopical measurements (different from TRLFS) can be used to determine the above mentioned parameters – UV-VIS (T_{00} and ω_{es},[d] spectrophotometric measurements are possible even for sub milimolar to micromolar total uranium concentration range when light absorbance is measured in a very long capillary (as is practiced at Helmholtz-Zentrum Dresden-Rossendorf (HZDR) [27]) and Raman (ω_{gs}), Excited state EXAFS (ΔR – from R_{es} if R_{gs} is measured by normal EXAFS). The IR spectroscopy would provide information on anti-symmetric stretching mode of the uranyl central group[e] (IR is possible only under special circumstances for aquesous samples, of course).

[a] For a preliminary investigation of several excited states of UO_2^{2+} and $[UO_2(H_2O)_5]^{2+}$ within explicitly relativistic Dirac-Coulomb-Gaunt Hamiltonian based methods, please see the Supplementary Information. The DIRAC 16 code for there presented calculations [18] has been used.

[b] or Fig. 15 in 4.4 in this contribution.

[c] The question of other vibrational modes contribution is investigated in Supplementary Information with the help of eZSpectrum software [101].

[d] ω_{es} corresponds to the distance between peaks (assigned to the same initial and same final (excited) electronic state, but different vibrational substates of the electronic states in question). The value fitted from absorption spectrum (e.g. ω_{es} = 708 cm^{-1} for $[UO_2(H_2O)_5]^{2+}$ from [26]), however, might be different from the value determined through TRLFS (or fluorimetric) hot-band maxima fit since the initial state in luminescence might be different from the final state active in UV-VIS absorption spectrum.

[e] For a bare UO_2^{2+} in vacuum the symmetric and anti-symmetric vibrational mode frequencies have fixed ratio (for derivation, see [28] (just change $^{12}C \rightarrow {}^{238}U$)),

Spectroscopic property derived from temporal domain is the luminescence lifetime, τ_m [ms] (under cryogenic conditions is in the ms range, unlike the μs range corresponding to the ambient conditions). Each species is characterized by a single τ_m value (m is the index of chemical species) parametrizing the simplest monoexponential luminescence decay model. However, the τ_m value even for a fixed species may vary from sample to sample because of different concentrations of quenchers (Cl^- [13], Fe^{2+}, Mn^{2+} [14] and organic compounds [2,15-17]) and/or different major species chemical composition (see eq. (21) and (22) in [1]). This is addressed as „matrix effect“ and can, to some extend, affect spectroscopic parameters derived from (emission) wave-length/wave-number domain (T_{00}, ω_{gs}, ω_{es}, ΔR, FWHMs) as well. The luminescence life-times are also dependent on temperature (approximately by an Arhenius Law for k_q parameters in eq. (22) of [1]) and matter phase (different in amorphous ice and liquid water even for the same temperature).

Interestingly, measureable changes in T_{00} and ω_{gs} of the same individual chemical components (UO_2^{2+}, UO_2SO_4, $UO_2(SO_4)_2^{2-}$ and $UO_2(SO_4)_3^{4-}$) have been detected between ambient and cryogenic conditions for uranyl – sulfate system (which has been measured under both conditions in one experimental campaign by author recently (the results will be published in near future) at HZDR). This phenomenon has been well known to other experimentalists at HZDR as well [29]. Unfortunately, such a comparison, is not possible for uranyl – carbonate system since uranyl carbonates yield insufficient luminescence under ambient conditions. However, some of the experience learned on the uranyl – sulfate system “ambient vs. cryo” comparison will help to answer questions such as “Is the speciation (un)changed in the process of cryogenic cooling of the sample?”. The general hope is that change is either small or predictable (and therefore, by thermodynamics based calculation correctable) and I will address this topic in my future contributions.

2.2 Multilinear experimental data analysis methods used – FATS and PARAFAC

2.2.1 Problem formulation

Since uranium total concentration in all studied samples is well below 0.003 mol.dm^{-3} (more concentrated solutions may exhibit self-absorption and luminescence signal might not be linear with respect to individual component concentrations), laser pulse energy has been around 1000 μJ only and MCP chosen so measurement has been done inside the linear part of dynamic range of ICCD detector, we can write measured luminescence signal in i-th spectrum, $Y_i(\lambda)$, as a linear combination of (yet unknown) TRLFS spectra from individual chemical species,

$$Y_i(\lambda) = \sum_{m=1}^{b} C_{im} Z_m(\lambda) + n_i(\lambda), \quad (3)$$

where λ is wavelength, C_{im} luminescence amnout in i-th spectrum corresponding to m-th species (individual component) and Z_m spectrum of the individual chemical species (e.g. UO_2^{2+}, UO_2SO_4, UO_2CO3, $Ca_2UO_2(CO_3)_3^0$, $CaUO_2(CO_3)_3^{2-}$, $MgUO_2(CO_3)_3^{2-}$, ..., m is a positive integer corresponding to some of the above written species). The total number of distinguishable components is denoted as b, $n_i(\lambda)$ is the noise function. The spectrum index i can either represent given i-th delay t_i between laser excitation of a sample and ICCD camera luminescence signal collection (case of kinetic/time series (TS) as in FATS) or given i-th sample (when delay is kept constant for all samples), or in the most robust procedure, there can be mapping between index i values and doubles (t, k), where t represents delay and k sample number (all kinetic series analyzed together).

The most general multilinear fitting procedure based on Singular Value Decomposition (SVD) [30-36,43,3,5,50,51] can be formulated as follows:

let us assume that from SVD decomposition of measurement data matrix Y_{li} (spectral index $i \in \{1,2, \ldots, s\}$, wave-length index $l \in \{1, 2, \ldots, N\}$),

$$Y_{li} = \sum_j U_{lj} W_{jj} V_{ij}, \quad (4)$$

or in matrix form

$$Y = U W V^T, \quad (5)$$

we take first f components ($j \in \{1, 2, \ldots, f\}$) as representing signal and filter out the remaining components ($j > f$).

Matrix U in (5) has orthonormal columns (and same dimensions as the original data matrix Y, the columns of U are called “subspectra”, the first f of them represent orthonormal basis of subspace of R^N corresponding to signal spectra), matrix W is diagonal positive semi-definite with diagonal elements (“singular values”) sorted from the greatest to the smallest and V columns are called “loadings”, they form an orthonormal set and j-th loading elements V_{ij} represent relative amount of j-th subspectrum in i-th original spectrum. Again we can think about columns of V (loadings) as basis vectors (in R^s, space of different concentration/amount profiles of individual chemical species). Filtering out noise-like small components mentioned in previous paragraph means that in later derivation only first f columns are considered for matrices U and V and that only first f x f diagonal block of W is considered as well.

$$\frac{\omega_{antisym,j}}{\omega_{sym,j}} = \sqrt{1+2\frac{m_O}{m_U}} \doteq 1.065, \quad (2)$$

which approximately holds even in presence of ligands and solvent as long as both symmetric and anti-symmetric stretching modes are well defined.

Setting (5) equal to matrix variant of (3), which reads

$$Y = Z C^T + E, \quad (6)$$

and using Ansatz

$$Z = U R^T, \quad (7)$$

will lead to matrix equation

$$V = CRW^{-1}, \quad (8)$$

entering fitting procedure described in detail later. The f x f square matrix R has yet unknown elements (which will be retrieved by the fit of (8)) and represent transition matrix between orthonormal basis of subspectra and nonortogonal set of (yet unknown) individual component spectra.

In general, we can consider gaussian likeli-hood functions [37-42] for loadings V_{ij} (assumed to be statistically independent and random gaussian distributed around modelled average) variables (8), leading to problem of minimization of the objective function

$$\chi^2_{MLM}(R,\beta,\gamma) = \sum_{i,j} \frac{\left(V_{ij} - C^{(\mathrm{model})}_{im}(\beta) R_{mj} W^{-1}_{jj}\right)^2}{\sigma^2_{ij}(\gamma)} + \sum_{i,j} \ln\left(\sigma^2_{ij}(\gamma)\right), \quad (9)$$

where summation is over $i \in \{1,2, \ldots, s\}$ and $j \in \{1,2, \ldots, f\}$, σ_{ij}^2 stands for variance of V_{ij} and γ for a set of parameters of dependence σ_{ij}^2 on V_{ij}, for Poisson-like distribution model, we can consider

$$\sigma^2_{ij}(\gamma_j) = \gamma_j \cdot \underset{l}{\mathrm{mean}} |Y_{li}|, \quad (10)$$

and $C^{(\mathrm{model})}_{im}$ stands for model of luminescence amount „profile“ in studied spectra.

2.2.2 SVD-based methods and models

Three different cases should be considered:

1) FATS (Factor Analysis of Time Series, [3,5,7,30,33]) analysis (The s spectra represent one TRLFS kinetic series measurement of one separate sample, to each i correspond given delay t_i), then $C^{(\mathrm{model})}_{im}$ corresponds to the model of luminescence decay and for the most simple one, monoexponential, the parameters β are labeled τ_m and correspond to

$$C^{(\mathrm{model})}_{im} = \Omega_m \exp\left(-\tau_m / t_i\right), \quad (11)$$

where Ω_m is a prefactor corresponding to non-zero width of ICCD detector integration window (Δt, integration time). For single FATS analysis, Ω_m (12) can be omitted.

$$\Omega_m = \tau_m \left(1 - \exp\left(-\Delta t / \tau_m\right)\right). \quad (12)$$

2) FACSC (Factor analysis connected to speciation computation, [5,7,43,50,51]) – in this case the s spectra correspond to s different samples measured within one fixed delay and $C^{(\mathrm{model})}_{im}$ represent speciation model (i.e. (implicit) formula for m-th species molar concentration in i-th sample (i can be linked to i-th total ligand concentration $c_{L,i}$ or similar variable)). The parameters in this model can be, e.g., speciation/chemical equilibrium constants characterizing stability of individual components.

$$C^{(\mathrm{model})}_{im} = C^{(speciation)}_m \left(\beta^{spec}_m; c_{L,i}\right), \quad (13)$$

3) FATSCSC (Robust method extracting simultaneously information from temporal and concentrational domains, i.e. taking all kinetic series from all samples together, [5,7,43]). This method is more general and theoretically more powerful than PARAFAC as it allows for both „matrix effect“ incorportation via having whole matrix of life-time parameters $\tau_{m,k}$, where m stands for species and k for sample. Index i here corresponds to doubles (t_i, k). Expression for modelled luminescence amount is product of (11) and (13). The factor Ω_m (12), unlike for FATS, shouldn't be omitted here (as it depends on life-time $\tau_{m,k}$ which change with k and therefore with i).

$$C^{(\mathrm{model})}_{im} = C^{(speciation)}_m \left(\beta^{spec}_m; c_{L,k}\right) \cdot \Omega_{im} \exp\left(-\tau_{m,k} / t_i\right). \quad (14)$$

2.2.3 χ^2 minimization procedure [3,7]

The objective function χ^2_{MLM} can be minimized with constrains when neccessary (e.g. in case of multicomponent analysis of noisy spectra), the constrains can be put on [3,50]

i) Individual component spectra (usual constrain should be positivity evaluated in small set of spectral points – this leads to linear inequality conditions on rows of variable matrix R)
ii) C-model parameters (usual constrain should be for life-times τ_m, or speciation constants β_m to be positive or from given interval).
iii) Variance model parameters γ (positivity)

iv) Less usually, the "projected" or „true" luminescence amount profiles C_{im} should be constrained to be positive. C_{im} are evaluated via

$$C = VWR^{-1}, \quad (15)$$

Since (15) is non-linear in R_{mj} original variables, this constrain will lead to series of non-linear inequalities partitioning candidate set/space of parameters (R,β,γ) into several components of continuity.

In the most simplified version, the model of σ_{ij}^2 variance is fixed within minimization and the second, logarithmic term, in objective function (9) can be omitted. This corresponds to an usual χ^2-minimization.

Please note the difference between $C_{im}^{(\mathrm{model})}$ and C_{im} as those elements have in general different values, former corresponding to fitting function value, latter to measurement outcome.

Note should be made on the relationship between the considered factor dimension f and number of individual components b. In an ideal case $f = b$, matrix R is square and (in an ideal subcase) regular. But there is possibility to consider b individual component spectra to be expanded into f subspectra, with $f > b$. In that case R is rectangular and matrix inversions in formulae above have to be taken as pseudoinverses [44-49]. In the limit $f = s$ and without constrains this leads to simple spectral "deconvolution" [50,51].

2.2.4 Individual component spectra normalization

Pre-last note on the three (1), 2), 3)) SVD-based methods should be made on normalization of individual component spectra obtained from R matrix elements (7).

a) FATS and PARAFAC: norm of Z columns ($Z_m(\lambda_l)$, m fixed) corresponds to „luminescence amount" emitted by m-th component and will be denoted $\zeta_{k,m}$ (in case prefactor Ω_m is considered in the model (11), $\zeta_{k,m}$ has dimension s^{-1} (counts per second)). The $\zeta_{k,m}$ is a product of molar concentration[f] $C_{k,m}$ [mol·dm^{-3}] and „molar luminescence" μ_m [s^{-1}·mol^{-1}·dm^3] of a given species,

$$\zeta_{k,m} = \mu_m \cdot C_{k,m}. \quad (16)$$

It is not possible to conclude the two factors on left side of (16) separately.
It might be possible if $s > b$ samples with the same b species would be analyzed and least-square fitting of series of (16) equations (for different k and m) would be done (based on assumption that molar luminescence for the same species m is independent on solution index k[g]), but author has rather negative experience with such a fit, except $s >> b$ [3,5].

b) FACSC and FATSCSC: norm of Z columns corresponds to molar luminescence directly. These methods provide direct access to molar concentrations of chemical species in question.

The choice of norm is discussed in 2.2 section of [1]. The raw spectra $Z_m(\lambda)$ (or $Z_m(\nu)$ when considering the wave-number, ν, scale cm^{-1}) are divided by their norms to provide normalized individual component spectra $Z'_m(\nu)$[h]. Their further processing will be discussed in later section 2.2.6

The data preprocessing preceding the SVD and question of factor dimension, f, choice will be briefly addressed inside the experimental data analysis section.

2.2.5 PARAFAC

Parallel Factor Analysis (PARAFAC) in this study provide decomposition of order=3 data tensor[i] $Y(\nu,t,k)$ (from all kinetic series of all samples together) according to equation (minimizing norm of ε tensor there)

$$Y(\nu,t,k) = \sum_{m=1}^{N} Z_m(\nu)\cdot D_m(t)\cdot C_m(k) + \varepsilon, \quad (18)$$

where ν is wave-number, t delay and k sample index. The total number of signal component N is free parameter of the method, but can be decided by numerous diagnostics, among them, core consistency, CORCONDIA, available in MATLAB code should be noted. e is deviation which is minimized by the PARAFAC fitting procedure, m index components which are ordered by total luminescence amount connected with them (e.g. D_m could be normalized that $D_m(t_1) = 1$, $Z_m(\nu)$ that euclidean norm is 1 and total luminescence amount of m-th component can be expressed as a norm of $C_m(k)$ profile).

[f] $C_{k,m}$ here is different quantity than $C_{i,m}$ in (11) or (15). In (11), we consider time-dependent (hence index i, for FATS parametrizing temporal domain, via $i \to t_i$) concentration of excited state (of species m). But in (16) molar concentration of the respective species m is denoted $C_{k,m}$ (hence index k denoting solution) – i.e. time-independent constant.

[g] And that some additional information is known, here it could be a total uranium concentration. Then,

$$c_k^{(U,\mathrm{tot})} = \sum_m \frac{\zeta_{k,m}}{\zeta_m^{(\mathrm{molar})}}, \quad (17)$$

for $k \in \{1, 2, \ldots, s\}$ for $s > b$ is, in principle, ready for Σ (LHS-RHS)^2 fit with variables μ_m to be determined (and subsequent use in (16) to determine $C_{k,m}$ from $\zeta_{k,m}$).

$\zeta_{k,m}$ (and μ_m) contains device-dependent prefactor (independent on m and k) and only their ratios are comparable across literature.

[h] The primes are later dropped and „normalized" is omitted in naming as long as it is not important in particular.

[i] The terms 3-way data or 3-mode data is also widely used in chemometrics. The PARAFAC method can be formulated also for M-way data when $M > 3$.

In contrast to SVD-based methods listed in 2.2.2, PARAFAC need neither model of luminescence decay nor speciation model as an input. It is widely known and well utilized method available in several different software implementations and could be therefore used almost as a black-box. This makes it method of the first choice for several preliminary data analysis.

However, aside of the „matrix effect" neglection drawback discussed already in 2.2.2 (point 3)), there is another one – PARAFAC, in its original formulation, needs kinetic series of all samples to be measured with exactly the same temporal point choice (even if some samples exhibit only short-lived luminescence and some long-lived only). This is not case of FATSCSC. For a deeper analysis of compliacted systems, PARAFAC results should be taken with caution and rather as second to FATSCSC or FATS results.

2.2.6 Individual component spectra fitting and further analysis

The (normalized) individual component spectra has been fitted to linear combination of seven gaussian peaks (indexed by index n, which can be interpreted as difference between vibrational quantum numbers of $p' \rightarrow p$, $n = p - p'$ in the simplest model either $p' = 0$ or $p = 0$ and $n \geq 0$ corresponds to cold bands and $n < 0$ to hot bands),

$$Z'_m(\nu) = \sum_{n=-N_h}^{N_c} c_{n,m}^2 \exp\left(- \frac{\left(\nu - \nu_{n,m}\right)^2}{2\sigma_{n,m}^2} \right), \quad (19)$$

where $\nu = 1/\lambda$ (connecting $Z'_m(\nu)$ and Z'_{lm} notation) is wave-number, summation limits are $-N_h$ (N_h being number of hot-bands) and N_c (number of cold-bands), $c_{n,m}^2$, $\nu_{n,m}$ and $\sigma_{n,m}$ are n-th peak height, maximum and variance parameter respectively. Gaussian fits has been done via routine in Wolfram Mathematica [100].

Subsequently, peak maxima are correlated with their number n according to formulae

$$\nu_{n,m} = T_{00,m} - \omega_{gs,m} \cdot n, \quad (20)$$

$$\nu_{n,m} = T_{00,m} - \omega_{es,m} \cdot n. \quad (21)$$

Area under n-th peak according to (19)

$$S(n) = \sqrt{2\pi}\, \sigma_{n,m}\, c_{n,m}^2, \quad (22)$$

could be used to determine ΔR_m through fitting to linear harmonic oscillator Franck-Condon factor [52-55] ratio as suggested in [1] (page 5).

For single mode linear harmonic oscillator Franck-Condon factor explicit formula (23) from [56] has been used. In following formula (23) in this study, simplified version for vibrational quantum number $\nu = 0$ has been used (with ν' any natural number), i.e.

$$2^n n! \cdot \left|\left\langle 0;\omega,R \middle| n;\omega',R' \right\rangle\right|^2 = \left(\sum_{k=0}^{\lfloor n/2 \rfloor} \binom{n}{2k} \left(\frac{4\omega}{\omega+\omega'} \right)^k (2k-1)!!\, H_{n-2k}\left(-\Omega\, \omega^{-1/2} d \right) \right)^2, \quad (23)^{j}$$

with

$$\Omega = \frac{\omega+\omega'}{\omega'\omega}, \quad (24)$$

where $\left|\left\langle 0;\omega,R \middle| n;\omega',R' \right\rangle\right|^2$ is the Franck-Condon factor ($\Delta R = |R-R'|$, ω and R are shown to stress that bra and ket vectors from this expression are not dual to each other except for $R=R'$ and $\omega=\omega'$ case). For setting $\alpha = \omega_{gs}$, $\alpha' = \omega_{es}$ (or in reverse order for hot bands) in (23) [56], the variable $d = C \cdot \Delta R$, where

$$C^2 = \frac{\mu m_u c}{\hbar}, \quad (25)$$

where c is speed of light in vacuum, m_u atomic mass unit (Dalton) and μ reduced mass of vibrational mode in question (here the symmetric stretching mode of uranyl group, i.e., $\mu = m(^{16}O)$ for the most common isotopologue $^{238}U^{16}O_2^{2+}$).

2.2.7 Two or one hot band? Interpretation questions

Since the differences between wgs and wes are even smaller than the ~160 cm^{-1} for $[UO_2(H_2O)_5]^{2+}$ [1] (for $M_nUO_2(CO_3)_3^{2n-4}$ (M = Ca, Mg), the difference $\Delta\omega$ can be less than 50 cm^{-1}), it is hard to determine the crossing point of the two linear branches on peak maximum = f(peak number) curve and therefore decide whether studied luminescence spectra exhibit one hot band (and T_{00} ~ 20 000 cm^{-1}) or two hot bands (and T_{00} ~ 20 800 cm^{-1} differ by one vibrational quantum $\omega_{gs} \sim \omega_{es}$ ~ 800 cm^{-1}). The impact to goodness of fit according to Franck-Condon factor formula (23) is greater and the two hot bands model have been found as better consistent with experimental data.

For comparison, the uranyl – sulfate system TRLFS spectra measured under ambient conditions exhibits one hot-band only [6]. Why would cryogenic conditions lead to greater number of hot bands (and much greater portion of luminescence emitted in the hot band peaks)? The possible answer might be that deexcitation in solid phase sample doesn't enter „thexi"[k] [62] stage as in liquid case and vibrationaly excited substates of electronic excited state are therefore stabilized. To assure both two hot band interpretation and theoretical explanation of its origin, series of TRLFS measurements on uranyl – sulfate

[j] This formula can be further generalized for the case of general 3N-5 or 3N-6 mode harmonic oscillator systems [57,58] under the Duschnisky mixing effect [59-61] (N is number of atoms in studied molecule).

[k] Thermally Equilibrated Excited (electronic) State.

system in both aqueous solutions and ice under several different temperatures should be done.

2.2.8 Identification of given chemical species – individual component assignment problem

Neither FATS nor PARAFAC could provide us with definite answer on chemical composition of samples in question alone. After the data analysis, we are left with a list with rows τ_m, ζ_m, ($T_{00,m}$, $\omega_{gs,m}$, …) for $m \in \{1, 2, …, f\}$ only. The interpretation to which chemical species $m = 1$, $m = 2$, …, $m = f$ components correspond is yet to be done. There are several possibilities for the above mentioned assignment:

a) Literature search for experimental spectra
b) Experimental speciation study (cryo-TRLFS measurement on series of artificial samples (solutions made from pure chemicals as UO_3, Na_2CO_3, Na_2SO_4, $CaSO_4$, …))
c) Quantum-chemical modelling (self-made or literature search).
d) By comparison of PARAFAC obtained luminescence-speciation and geochemical model (provided, e.g. by PhreeqC modelling based on existing thermodynamic properties database).

3 Experimentals

3.1 Sample characterization

Samples orginated from a flooded uranium mine prior (S1) and after water treatment (S2) and from seepage water of uranium processing tailings management facilities (TMF's; S3 – S5, S9).

Samples S5 and S4 have been created by hydrochloric acidification of sample S3 to pH = 6 and 5.5, respectively to investigate acidification driven speciation change.

Table 1 gives total elemental concentrations in mg/l, *pH* and E_H in mV, sample number is written in the first row. S(VI) stands for sulfate SO_4^{2-}, C(IV) for hydrogencarbonates (bicarbonates) HCO_3^- and carbonates (CO_3^{2-}, except for S9 almost all C(IV) is in the form of HCO_3^-), N(V) for NO_3^-.

Table 1: Total elemental conc. (mg/l, adopted from [66])

E \ S	1	2	3	4	5	9
Na	121	122	1350	1550	1580	2520
K	12.8	12.8	27.4			
Mg	104	100	301	333	340	61.8
Ca	158	191	292	296	302	86.5
Fe	5.09	0.18	0.28			0.08
Mn	2.17	1.4	0.482			
U	1.68	0.02	3.1	3.38	3.53	10.8
Cl	54.3	452	496	908	815	1170
S(VI)	576	546	3620	4030	4100	3150
C(IV)	574	14	657	113	300	2244
N(V)	<0.5	<0.5	3.6			
pH	7.1	7.4	7.3	5.5	6	9.3
E_H	130	450	310	310	310	400

3.2 Measurement

The measurements have been done by HZDR collective [66]. Briefly, samples have been cooled by liquid nitrogen into solid ice-blocks inside plastic cuvette and then placed into cryostat set to (-120±2)°C (Cool gas system TG-KKK produced by KGW). After 15 minutes for temperature equilibration, Time-Resolved Laser-Induced Fluorescence Spectra (TRLFS) has been recorded with pulse energy 1 mJ, excitation wave-length 266 nm and pulse duration 2 ns. Emission wave-length measurement range has been set to 450-650 nm. Minilite Laser System (produced by Continuum) with Spectrograph and ICCD-camera iHR 550 (HORIBA Jobin) has been used. For the spectra recording, software LabSpec has been used [65].

Emission wave-length sampling corresponded to average step of $d\lambda = 0.463$ nm (i.e. $d\nu = 18.5$ cm^{-1} for $\nu = 1/\lambda = 20000$ cm^{-1}). Time series (series of spectra differing by time interval t_i between laser excitation and start of emission spectra recording) consistend of three types – short („D2", $s = 41$ points, $dt = 0.05$ ms, i.e. $t_{41} = 2.001$ ms), long („D3", $s = 51$ points, $dt = 0.1$ ms, i.e. $t_{51} = 5.001$ ms), very long („D4", $s = 100$ points, $dt = 0.101$ ms, i.e. $t_{100} = 10$ ms). Sample S1 has been measured with D3 temporal sampling, samples S2, S3, S5 and S9 with D2+D3 sampling, sample S4 with D3+D4 sampling.

For PARAFAC data analysis D3 sampled kinetic series from samples S1-S5 and S9 have been the input.

4 Data analysis of Experimental results

4.1 FATS computationals

The SVD decomposition as described in 2.2.1-2.2.3 has been applied with weighting-preprocessing[1] [3,5,7,50,51] such that original measurement data matrix elements Y_{li} has been transformed onto Y'_{li} normalized data matrix via

$$Y'_{li} = \frac{Y_{li}}{P_l Q_i}, \tag{26}$$

where $P_l Q_i$ represent separable form of variance of Y_{li}, so Y'_{li} are now closer to case of independent and identicaly distributed random variables. Since greater variance lies along temporal domain, P_l can be set as $P_l = 1$ and Q_i has, in software MyExpFit V4 [98] (used for all FATS computations, written in Matlab [99]), general form

$$Q_i = \underset{l}{mean} \left| Y_{li} \right|^{\phi}, \tag{27}$$

where $\phi \in (0;1)$. For purely poisson noise, $\phi = 0.5$, this choice has been applied here. After SVD procedure (4), (5), $Y' = U' W V'^T$, the subspectra and loadings should be „denormalized" back according to formulae below,

[1] The term NmSVD is used then (Nm = **N**or**m**alized).

$$U_{lj} = U'_{lj} P_l, \quad (28)$$

$$V_{ij} = V'_{ij} Q_i. \quad (29)$$

The factor dimension f can be, in general case, determined according to three different diagnostics [3,5,7,50,51]:

i) SCREE-plot diagnostics [63,64] focus on crossing of linear branches in log $W_j = f(j)$ plot (Fig. 1). On example for sample S3, $f = 3$ or $f = 4$ since the last branch with smallest slope corresponds to noise, but from SCREE-plot alone it is hard to recognize whether still to include $j = 4$ component or not.

ii) Loadings-based V-diagnostics focus on number of first, signal-like, loadings. For S3 sample, Fig. 2 and Fig. 3 show three signal-like loadings. Since fourth, loadings are much more noise-like (Fig. 4).

iii) Subspectra-based U-diagnostics works as previous, except for subspectra. Fig. 5 presents first three signal-like subspectra, Fig. 6 subspectrum U_4' already noise-like.

While ii) and iii) diagnostics for the chosen example (Sample S3 TRLFS kinetic series analysis) suggest to accept $f = 3$ components for further analysis, it is better just to conclude that it is possible to statistically distinguish $N = 3$ independent luminescence active species (according to the geochemical modelling it should be $Ca_2UO_2(CO_3)_3^0$, $CaUO_2(CO_3)_3^{2-}$ and most probably $MgUO_2(CO_3)_3^{2-}$), but set $f = N + 1 = 4$.

Because the software based background correction/subtraction [65] is rather approximate, irrespectively to method free parameter choice, FATS for $f > 2$ provide one individual component with several orders of magnitude larger life-time (and smaller luminescence amount) and bandless continuum-like luminescence spectrum. This component corresponds to background artifact and is ignored in further analysis. Therefore, for N chemical component model, $f = N + 1$ has to be chosen. By preliminary analysis of randomness of residuals, case $N = 1$ has been found as insufficient for any sample investigated below, $N = 2$ as a slight under-fit and $N = 4$ as a slight over-fit.

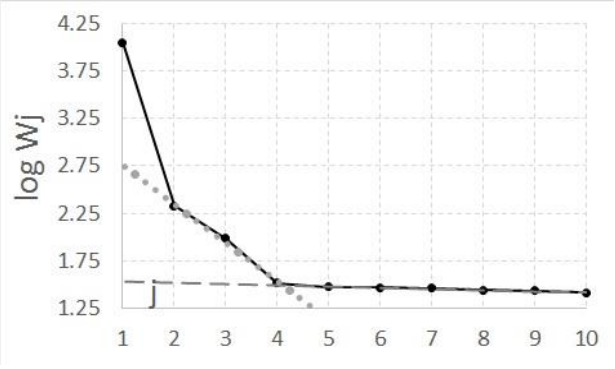

Fig. 1. SCREE plot for NmSVD of connected TRLFS kinetic series for sample S3. $W_j = W_{jj}$ is the j-th singular value, j on horizontal axis. The singular values are plotted as black circles connected by thick lines. Dashed and dotted lines correspond to linear approximation of $j = 5$ to 10 and $j = 2$ to 4 regions, respectively.

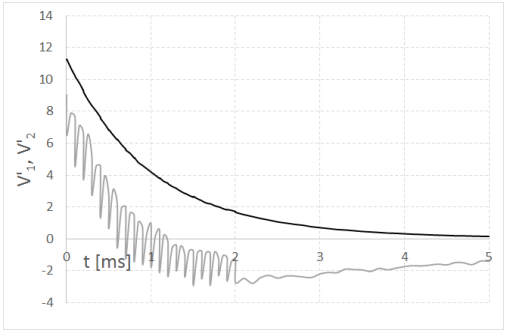

Fig. 2. NmSVD Loadings (sample S3) of the first two components ($j = 1$ (black) and $j = 2$ (gray)).

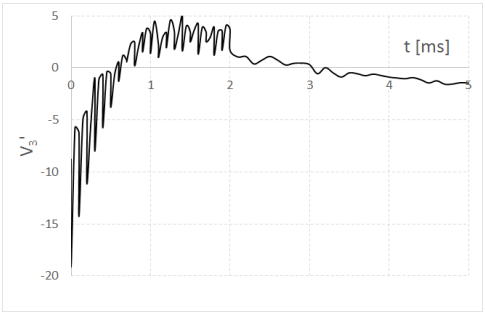

Fig. 3. NmSVD Loadings (sample S3) of third component ($j = 3$, still considered as signal).

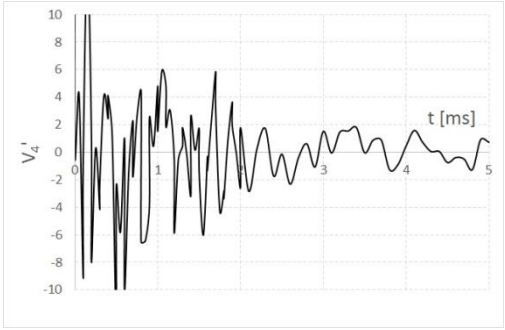

Fig. 4. NmSVD Loading (Sample S3) of fourth component – very noisy, represent background and noise. Last loading taken into further analysis.

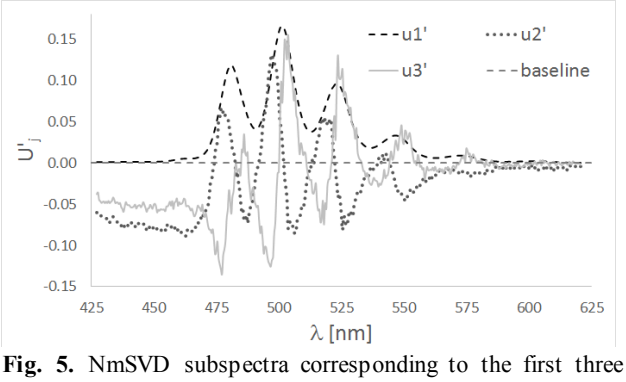

Fig. 5. NmSVD subspectra corresponding to the first three components ($j \in \{1,2,3\}$), clearly corresponding to subspace of

signal (in R^N, where N = 419 is number of spectral points selected).

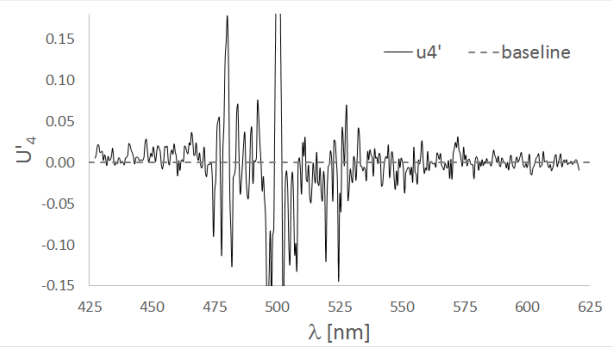

Fig. 6. First, NmSVD subspectrum U'_4 corresponding to noise has been added to further analysis for the need to represent background subtraction artifact, but subspectra for $j > 4$ are omitted from further analysis.

4.2 Sample S1 (mine water)

NmSVD for this sample suggest N = 3 (or 2) and therefore f = 4 (or 3) (Fig. 7). Denormalized f loadings from NmSVD has been fitted to linear combination of f exponential decays, resulting luminescence amounts ζ_m [10^3 ms^{-1}] and life-times τ_m [ms] are presented in Tab. 2.

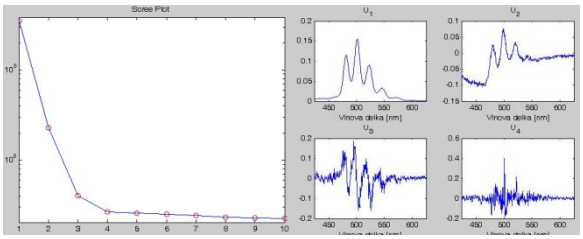

Fig. 7: NmSVD SCREE-plot and U-diagnostics done by MyExpFit V4 program [98].

FATS f = 3 and f = 4 analysis has been done. Resulting individual component spectra (Fig. 8, Fig. 9) in the former case contained "structure" inside the background component (dotted in Fig. 8) which favoured latter f parameter choice. Please note the peak maxima (e.g. for the highest peak) of the component differs by a tiny portion of 0.86 nm (less than twice of wave-length sampling period!) for f = 3 and ~ 1 nm (~ 50 cm^{-1} in this region) for the two charged complex species for f = 4 as well.

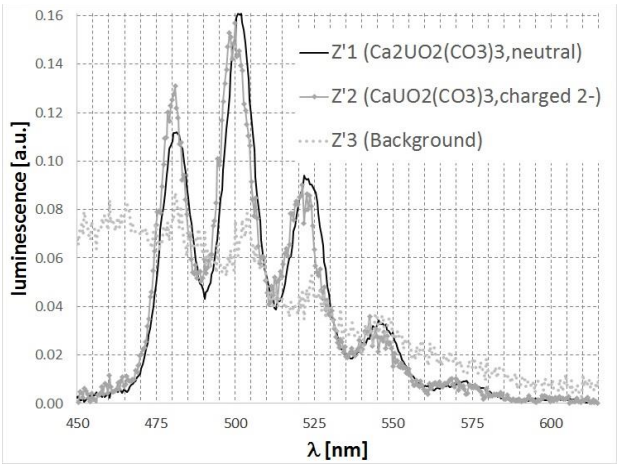

Fig. 8. FATS, f = 3 analysis of sample S1 results for individual component spectra (nm scale).

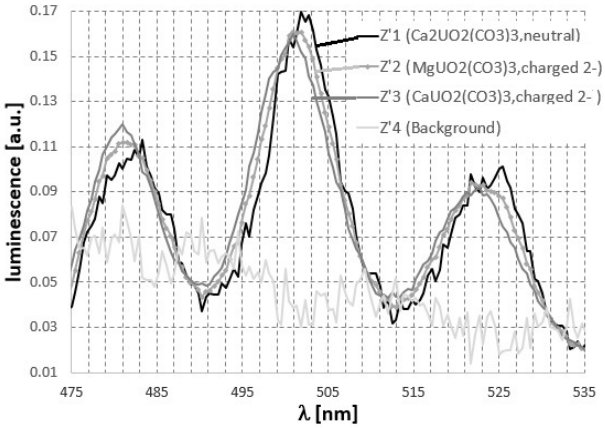

Fig. 9. FATS, f = 4 analysis of sample S1 results for individual component spectra (nm scale, for better visibility of peak position differences, only three largest peak detail is shown).

Spectroscopic parameters – T_{00} [10^3 cm^{-1}] (excitation energy) and ω_{gs} [cm^{-1}] (ground state vibrational frequency) have been calculated from gaussian fits of FATS f = 4 individual component spectra (Tab. 2, Fig. 10, 11 as an example for m = 1 component).

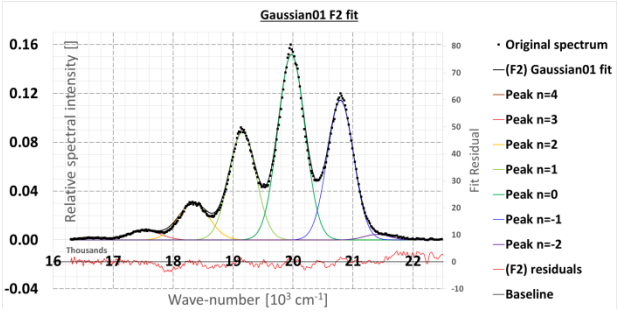

Fig. 10. m = 1, τ_1 = 0.87 ms component (assigned to $MgUO_2(CO_3)_3^{2-}$) of f = 4 FATS decomposed according to (19) (cm^{-1} scale).

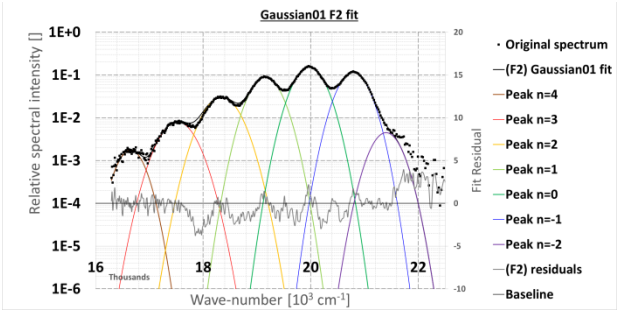

Fig. 11. $m = 1$ component ($f = 4$), intesity plotted in logarithmic scale to show approximate gaussian character for red-most and blue-most tiny peaks too.

For this sample, an example of ΔR estimation from experimental data is shown in Fig. 12 and Fig. 13, where one and two hot band models, respectively, have been used. In their comparison, two hot band model seems to be more realistic with $\Delta R = (7.3 \pm 1.0)$ pm

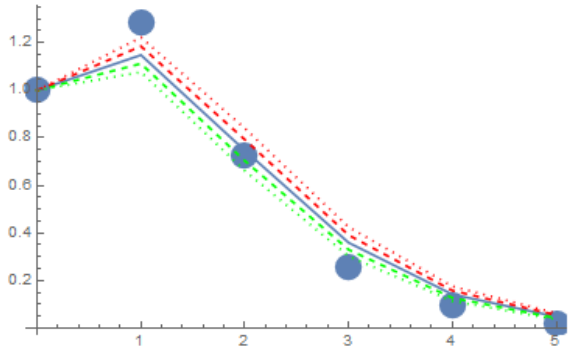

Fig. 12. FATS $f = 4$, $m = 0$ ($\tau_0 = 0.36$ ms, assigned to $CaUO_2(CO_3)_3^{2-}$) Franck-Condon fit (23) within „one hot-band" model. Fitted $\Delta R = (10.4 \pm 1.0)$ pm. On vertical axis, $n' \rightarrow 0$ peak area (22) relative to $0' \rightarrow 0$ peak is plotted. Horizontal axis represents vibrational number n'.

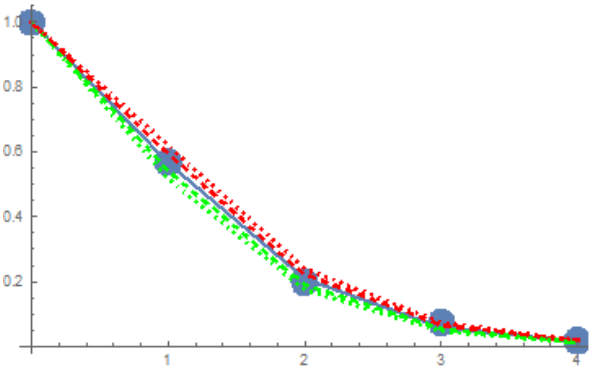

Fig. 13. FATS $f = 4$, $m = 0$ as in previous Fig. 11, but within „two hot bands" model. $\Delta R = (7.3 \pm 1.0)$ pm. The dashed lines corresponds to $\Delta R = (\Delta R)_{min} \pm 0.7$ pm, the dotted lines to $\Delta R = (\Delta R)_{min} \pm 1.3$ pm, where $(\Delta R)_{min}$ is the χ^2 fit optimum value.

Table 2: FATS $f = 4$ results for sample S1.

m	τ_m	ζ_m	$T_{00,m}$	ω_{gs}
0	0.36	8.1	20.01 ± 0.01	794
1	0.87	30.1	19.97 ± 0.02	816
2	1.52	4.51	19.92 ± 0.03	807
3	9.52	0.09	n.d.	n.d.

4.3 Sample S2 (treated mine water)

Same procedure as for S1 has been repeated, results are presented in Table 3 below (since now, background component is not listed). The uncertainities are $\delta(\omega_{gs})$ ~10cm^{-1}, $\delta(\tau_m)$ ~ 0.1 ms and $\delta(\zeta_m)$ ~ 0.2 ms^{-1}.

Table 3: FATS analysis results, sample S2 (treated mine water)

f	m	τ_m	ζ_m	$T_{00,m}$	ω_{gs}
3	0	0.45	2.57	19.98 ± 0.01	804
	1	1.15	2.53	19.94 ± 0.02	833
4	0	0.21	1.83	20.07 ± 0.04	798[m]
	1	0.76	2.38	19.97 ± 0.02	810
	2	1.26	1.55	19.92 ± 0.03	830

4.4 Sample S3 (TMF seepage water)

NmSVD and FATS as done for previous samples revealed following parameters (Tab. 4). Due to the higher uranium content, signal:noise ratio has been higher and smoother individual component spectra resulted (Fig. 14). An example of fitting procedure for T_{00}, and ω_{gs}, determination is presented in Fig. 15, the uncertainities are lower than in S1 by roughly factor of 2.

Table 4: FATS analysis results, sample S3 (TMF seepage water)

f	m	τ_m	ζ_m	$T_{00,m}$	ω_{gs}
3	0	0.81	93.2	19.98 ± 0.01	817
	1	1.39	36.9	19.93 ± 0.01	820
4	0	0.75	39.6	19.99 ± 0.01	810
	1	0.88	59.5	19.96 ± 0.01	817
	2	1.44	31.0	19.93 ± 0.01	819

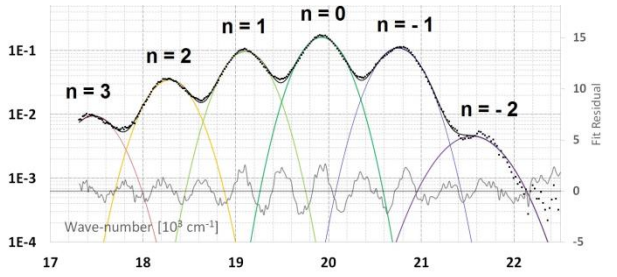

Fig. 14: FATS ($f = 4$), $m = 2$ individual component spectrum (later assigned to $Ca_2UO_2(CO_3)_3^0$) fitted to linear combination of gaussian profiles. Peak maxima has been fitted as a function of peak number n in follow Fig. 15.

[m] However after not one but two redmost peaks are excluded from the fit, $\omega_{gs} = 833$ cm^{-1} value results.

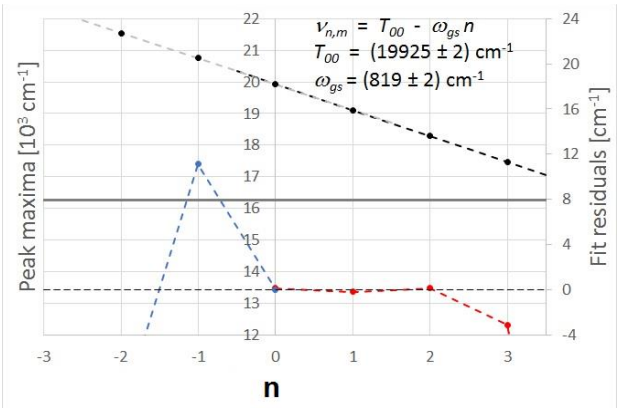

Fig. 15: Upper part: Peak maxima as peak number function (vertical principial axis in 10^3 cm^{-1} divides the two linear branches with almost identical slopes, the uncertainity of fit underestimates total experimental uncertainities), lower part: residuals of the fit (right axis in cm^{-1})

4.5 Sample S4 (acidified TMF seepage water)

FATS analysis for f = 4 of the sample created by acidification of S3 by HCl (to pH = 5.5) possibly revealed in previous samples not present component with both high T_{00} and ω_{gs} (m = 1, τ_1 = 1.15 ms), which might be either UO_2CO_3 or UO_2SO_4, but its small luminescence amount ($\zeta_1 \sim 0.07 \cdot 10^3$ ms^{-1}, Table 5) is in contrast with high relative content predicted by geochemical modelling for this acidified sample. Similarly, the component associated with τ = 0.84 ms (f = 3) or τ = 0.88 (f = 4) could be assigned to UO_2CO_3 (ω_{gs} = 815 cm^{-1}, T_{00} = 20080 cm^{-1} fitted from deep cryogenic measurements done in [67], τ = 0.47 ms) or UO_2SO_4 due to the previously reported luminescence life-time of UO_2SO_4 under cryogenic conditions of 0.4 ms.

Table 5: FATS analysis results, sample S4 (acidified TMF seepage water)

f	m	τ_m	ζ_m	$T_{00,m}$	ω_{gs}
3	0	0.83	36.9	19.99 ± 0.01	816
	1	1.34	24.3	19.92 ± 0.01	819
4	0	0.83	36.6	19.99 ± 0.01	815
	1	1.15	0.07	20.02 ± 0.02	827
	2	1.34	24.4	19.92 ± 0.01	819

4.6 Sample S5 (acidified TMF seepage water)

Following table 6 presents FATS results for the sample S5 created by acidification of S3 by HCl to pH = 6.0.

Table 6: FATS analysis results, sample S5 (acidified TMF seepage water)

f	m	τ_m	ζ_m	$T_{00,m}$	ω_{gs}
3	0	0.84	97.4	19.96 ± 0.02	816
	1	1.44	34.4	19.92 ± 0.02	820
4	0	0.59	6.81	20.06 ± 0.02	800?
	1	0.88	98.5	19.95 ± 0.02	816
	2	1.51	26.9	19.91 ± 0.02	830

Uncertainities of spect. param. are at least 20 cm^{-1} here.

4.7 Sample S9

Since Sample 9 had the highest total uranium concentration among all studied samples, individual component spectra from FATS analysis have been smoother than in previous samples (Fig. 16, 17) and excitation energy parameter T_{00} experimental uncertainities have been the lowest (Tab. 7).

Table 7: FATS analysis results, sample S9

f	m	τ_m	ζ_m	$T_{00,m}$	ω_{gs}
4	0	0.48	87.7	19.99 ± 0.01	799
	1	0.91	225.3	19.97 ± 0.01	806
	2	1.50	134.4	19.93 ± 0.01	807

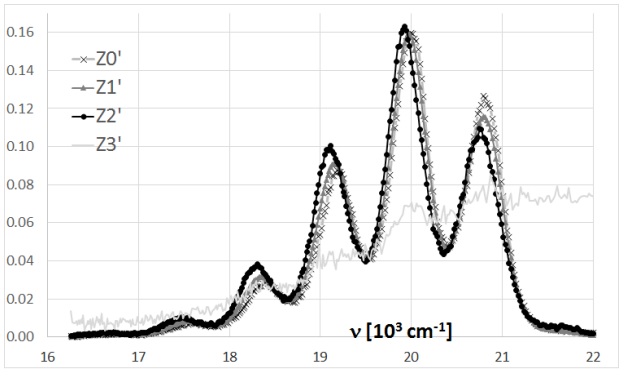

Fig. 16. Individual component spectra from FATS, f = 4 analysis, T_{00} decrease with increasing luminescence life-time t of components (ordered as $\tau_1 < \tau_2 < \tau_3 \Rightarrow T_{00,1} > T_{00,2} > T_{00,3}$).

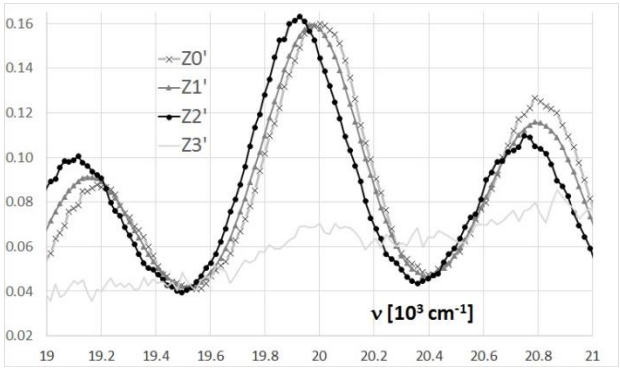

Fig. 17. Detail on three highest peaks in previous spectra.

4.8 PARAFAC analysis of all samples together

PARAFAC decomposition according to (18) led to luminescence amount profiles (Fig. 18), by maximizing objective function

$$f(\pi) \equiv \sum_{m=1}^{N} \left(\sum_{k=1}^{s} \Gamma_{k,m} M_{k,\pi(m)} \right) W_m , \qquad (30)$$

where $\Gamma_{k,m} = C_k(m)/\Sigma_n C_k(n)$ is relative luminescence amount of m-th component (18) in k-th sample, $M_{k,\pi(m)}$ is $\pi(m)$-th species concentration in k-th sample according to

geochemical modelling calculation [66] (Fig. 19, done in EQ3/6 [68] (default thermodynamic database data0.R2.com) in [66] and independently reproduced by PhreeqC [69] with a database input from NEA thermodynamic database [70] supplemented with parameters for $Ca_2UO_2(CO_3)_3^0$ [71] and $CaUO_2(CO_3)_3^{2-}$ [72]), W_m is weight, $N = 7$ (the background component is excluded) and maximization is done with respect to permutation π Resulting optimal assignment is presented in Table 8 and parameters τ[ms], T_{00} [cm^{-1}] and ω_{gs} [cm^{-1}] (from monoexponential fits of $D_m(t)$ and gaussian fits of $Z_m(\nu)$ (18)) should be compared to found literature experimental data (Table 9) and quantum chemical calculations (section 6).

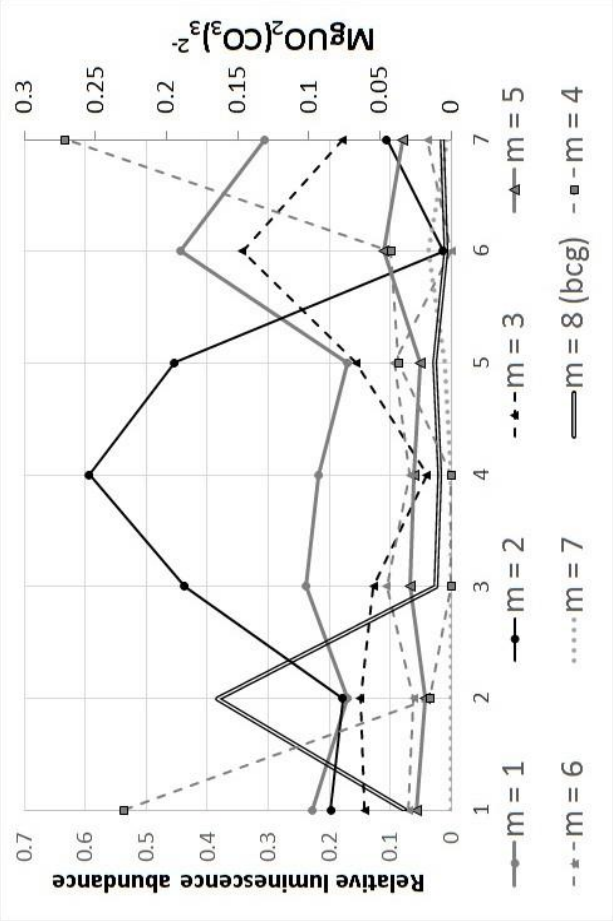

Fig. 18. Relative luminescence abundance linked to the m-th individual component of PARAFAC decomposition as a function of sample index (luminescence amount profiles).

Table 8: Optimal component assignement

m	Species	τ [ms]	T_{00} [cm^{-1}]	ω_{gs} [cm^{-1}]
1	$CaUO_2(CO_3)_3^{2-}$	0.551	20051	806.0
2	$Ca_2UO_2(CO_3)_3$	1.322	19916	823.4
3	$UO_2(CO_3)_3^{4-}$	1.001	19858	812.3
4	$MgUO_2(CO_3)_3^{2-}$	0.902	19973	797.1
5	UO_2CO_3	1.091	20089	816.9
6	UO_2SO_4	0.658	19970	831.4
7	$UO_2(CO_3)_2^{2-}$	1.044	19914	798.4

Table 9: Comparison with literature

m	$T_{00,REF}$	$\omega_{gs,REF}$	τ_{REF}	REF
1			0.615	[66][n]
2	19943	798 ;820	1.009	[73][o]
3	20007		0.887	[74]
5			0.905	[66][p]
	20081	815	0.465	[67][q]
6			0.400	[75]
7	20145	810	0.963	[67]

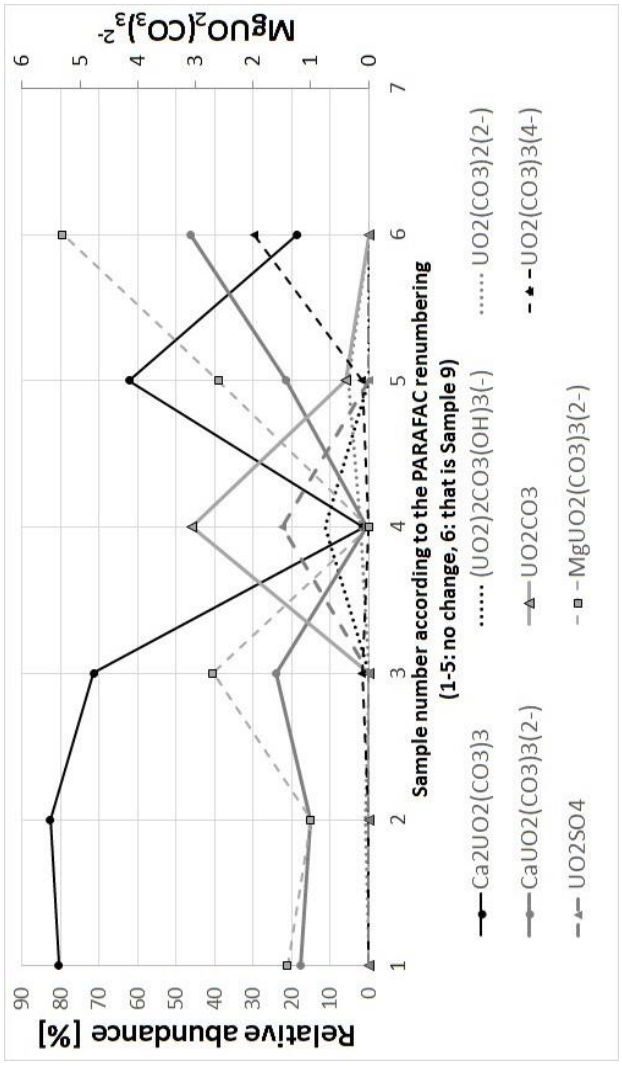

Fig. 19. Relative abundance of chemical species according to geochemical modelling calculation [66,68-72].

[n] Average from all life-times assigned to this species in Tab. 4 of [66].
[o] The higher reference value for luminescence life-time of 1.282 ms from [67] is even closer, but corresponds to much lower temperature of 6K.
[p] Here and in first line of Table 9, the comparison of life-time is made with respect to different analysis of the same data.
[q] This τ_m value correspond to a lower temperature of 6K. However, luminescence life-time should decrease with increasing temperature.

5 Computationals for quantum chemical calculations

Similarly to [1] calculations were done in Turbomole V6.5 program [78,94] on MetaCentrum computational grid system [98]. Scalar relativistic effects were approximately included via 60 electron Effective Core Potential (ECP) for uranium atom [79,80], all other electrons were, at this level of approximation treated as non-relativistic. Hydration has been described by explicit inclusion of small number (denoted *n* in chemical formulae like $[UO_2(\kappa^2\text{-}CO_3)(H_2O)_3]$. *n* H_2O) of water molecules into investigated system. The atomic basis sets used were def-SVP (denoted „S“ in all tables in the section 6 below, [78,79,81,82]), def-TZVPP (denoted „T“, [83], for solvated models, solvent water molecules only def-SVP atomic basis set was used to reduce the computational demands, denoted „Tc“ [1] or „def-TZVPPc“) and def-QZVPP (denoted „Q“ [95], for uranium at most def-TZVPP has been used).

For the ground state properties DFT/B3-LYP [84-86,93] has been used. For DFT calculations the D3 dispersion correction has been applied [91]. All figures have been exported from Molden [92] screenshots.

6 Quantum chemical calculation results

6.1 Uranyl Monocarbonate, UO_2CO_3

Similarly as for the uranyl monosulfate, UO_2SO_4, four different configurations should be investigated, differing by dentacity of CO_3^{2-} ligand (κ^2- for bidentate, coordinated by two donor oxygen atoms, κ^1- for monodentate, coordinated by one donor oxygen atom) and coordination number of central uranyl group UO_2^{2+} (i.e. number of water molecules coordinated to U along carbonate ligand), labeling from [1] will be adopted leading to κ^2co5 (for $[UO_2(\kappa^2\text{-}CO_3)(H_2O)_3]$), κ^2co6 ($[UO_2(\kappa^2\text{-}CO_3)(H_2O)_4]$), κ^1co5 (for $[UO_2(\kappa^1\text{-}CO_3)(H_2O)_4]$) and κ^1co6 (for $[UO_2(\kappa^1\text{-}CO_3)(H_2O)_5]$). In vacuum, only κ^2co5 has been found stable, explicit inclusion of water molecules allowed stabilization sligthly less stable κ^2co6 and when at least 18 water molecules has been added around studied complex, also κ^1co5. Ground state symmetric stretching mode frequency of uranyl group ω_{gs} and vertical (T_e, not T_{00}) excitation energies are reported in Table 10 below, where b. stands for atomic basis set, n for number of explicit water molecules (not coordinated to uranyl, but as solvent), *E* for relative energy (in mH for different b., in cm^{-1} if bold - for different local PES minima (b.,form and n identical), relative to closest most „0“ upside in the table), *R* for U-O_{yl} bond distance in pm.

Table 10: UO_2CO_3 prop. quant. chemical estimate.

ref	b.	form	*n*	*E*	T_e	ω_{gs}	*R*
1	S	κ^2co5	0	808	18808	873	179
2	T			38	18611	865	178
3	Q			0	18631	866	178
4	S	κ^2co5	12	**0**	20703	850	179
5	S		12	**3206**	20655	857	179
6	S		12	**3505**	20553	820	180
7	Tc		12	-874	20448	850	179
8	Tc		12		20250	813	180
9	*T*		*12*	*-1927*	*20394*	*856*	*178*
10	S		16	0	20695	865	178
11	Tc		16	-774	**20453**	**868**	178
12	S		25	0	21139	856	179
13	*Tc*		*25*	*-773*	***20863***	***852***	*178*
14	S	κ^2co6	12	**0**	20569	887	177
15	S		12	**1264**	20588	901	176
16	S		12	**1657**	20757	881	177
17	Tc		12	-872	**20328**	**886**	177
18	Tc		12	-862	20356	896	176
19	S		20			**861**	178

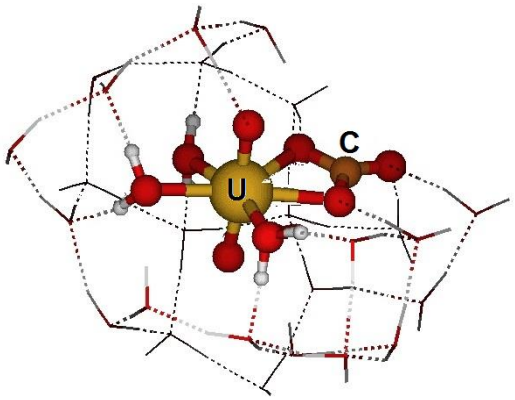

Fig. 20. At def-TZVPP/B3LYP/DFT-D3 level optimized geometry of $[UO_2(\kappa^2\text{-}CO_3)(H_2O)_3]$. 25 H_2O (solvent water molecules are represented by lines and def-SVP basis set us used for their description). Please note the planarity of CO_3^{2-} ligand situated in equatorial plane (approximately perpendicular to uranyl axis)

6.2 Uranyl bis(carbonate), $UO_2(CO_3)_2^{2-}$

Among all six possibilities only κ^{22}co5 isomer (supposed to be most stable) has been investigated. Results are presented in table below.

Table 11: Ground electronic state properties of $[UO_2(\kappa^2\text{-}CO_3)_2(H_2O)]^{2-}$ (U-O_{yl} bond length *R* in pm, vibrational frequency of UO_2^{2+} symmetric mode ω_{gs} [cm^{-1}]) and vertical excitation energies T_e [cm^{-1}].

ref	b.	*n*	*E*	T_e	ω_{gs}	*R*
1	S	0	0	20551	814	181
2	T	0	-905	20349	808	181
3	Q	0	-952	20355	810	180
4	S	12	0	20665	830	179
5	Tc	12	-893	**20507**	**827**	179

Aside of the vibrational frequencies in Tab. 11, there is also another mode with smaller contribution to uranyl symmetric streching with ω of 723, 710 and 710 cm^{-1} for ref. 1, 2 and 3 respectively.

For this molecule, electronic excited state PES local minima solution has been done and adiabatic energies T_a and T_{00} are presented together with deexcitation energy T_{de} [all in cm^{-1}] in the following table (ω_{es} is the symmetric stretching mode vibrational frequency of uranyl group in the excited electronic state in cm^{-1} and ΔR excitational elongation in pm).

Table 12: Excited electronic state properties of $[UO_2(\kappa^2\text{-}CO_3)_2(H_2O)]^{2-}$.

ref	b.	*n*	T_a	T_{00}	T_{de}	ω_{es}	ΔR
1	S	0	20075	19724	19532	677	3.9
2	T	0	19843	19542	19294	669	4.1
3	Q	0	19854		19312		4.1
4	S	12	20089		19442		

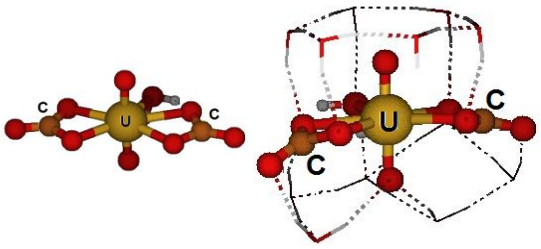

Fig. 21. Left: $[UO_2(\kappa^2\text{-}CO_3)_2(H_2O)]^{2-}$ in vacuum at def-QZVPP atomic basis set level, CO_3^{2-} ligands both planar and in equatorial plane, intramolecular H-bond, right: with 12 water solvent molecules around, carbonate ligands slightly out of equatorial plane.

6.3 Uranyl tris(carbonate), $UO_2(CO_3)_3^{4-}$

Uranyl tris(carbonate) molecule has D_{3h} point group symmetry. For some explicit solvated models the symmetry has been broken due to asymmetric surrounding by water molecules. Though no water is directly coordinted to the uranyl group, the explicit inclusion of solvent water molecules significantly change uranyl bond (U-O_{yl}) length R (the bond is shortened), frequencies of vibrational modes with symmetric U-O_{yl} stretching ($\omega_{gs,1}$ and $\omega_{gs,2}$ – by increasing them – as opposed to UO_2^{2+} hydration effect) and to a lesser extend (e.g. when compared to UO_2CO_3 or $UO_2(CO_3)_2^{2-}$) also vertical excitation energy T_e (Tab. 13).

Differences can be identificated between "sandwich-like" supramolecular complex containing 12 water molecules (six from each side in planes parallel to the coordination plane, Fig. 22) and 24 water molecular explicit hydrated structure (Fig. 23), where also all three non-coordinated ("terminal") oxygens of CO_3^{2-} ligands have been surrounded by three water molecules (allowing for partial stabilization of negative charge, Tab. 13) each.

Predicted adiabatic (T_a ~ 20 800 cm^{-1} – the value mentioned in theoretical background, Tab. 14) excitation energies for 12 water molecule solvated models would imply two-hot-bands interpretation of luminescence spectra. This is in contrast to uranyl bis(carbonate) model $[UO_2(\kappa^2\text{-}CO_3)_2(H_2O)]^{2-}$. $12H_2O$ (with a similar "sandwich-like" explicit water molecules surrounding), where T_a = 20 089 cm^{-1} ~ 20 000 cm^{-1} – the value mentioned in the theoretical background for one-hot-band interpretation. It would be interesting to see two luminescence spectra with similar band positions but "shifted" peak assignment to vibronic transitions[r]. Predicted vertical excitation energies, however, decrease with number of explicitly included solvent molecules and in inifity limit would drop to value closer to one-hot-band interpretation.

Table 13: Ground electronic state properties of $[UO_2(CO_3)_3]^{4-}$ (U-O_{yl} bond length R in pm, vibrational frequency of UO_2^{2+} symmetric mode ω_{gs} [cm^{-1}]) and vertical excitation energies T_e [cm^{-1}].

ref	b.	*n*	*E*	T_e	$\omega_{gs,1}$	$\omega_{gs,2}$	*R*
1	S	0	0	22104	780	724	183
2	T	0	-1165	21765	778	714	182
3	Q	0	-1234	22453	780	715	182
4	S	12	0	21434	**829**	720	179
5	Tc	12	-1122	**21217**	**838**	712	179
7	S	24	0	21290	**867**		178
8	Tc	24	-1106	**21068**	**863**		178

Table 14: Excited electronic state properties of $[UO_2(CO_3)_3]^{4-}$

ref	b.	*n*	T_a	T_{de}	ΔR
1	S	12	20862	20258	4.2
2	Tc	12	20670	20092	3.9

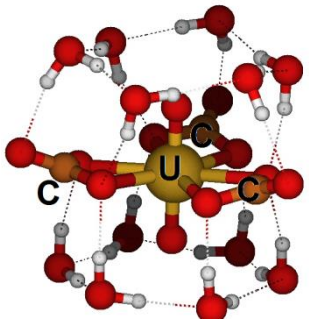

Fig. 22. „Sandwich-like" structure of $[UO_2(CO_3)_3]^{4-} \cdot 12\ H_2O$ (def-TZVPPc level).

[r] (e.g. current estimates would suggest 0'→0 of bis(carbonate) close to 0'→1 of tris(carbonate), 0'→1 of bis(carbonate) close to 0'→2 of tris(carbonate)).

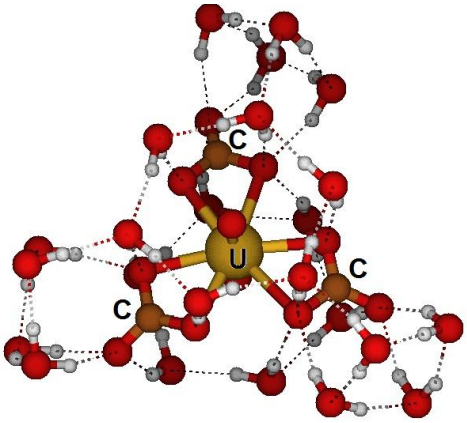

Fig. 23. Struct. corresponding to ref. 8 in Tab. 13.

6.4 Ternary complex $MgUO_2(CO_3)_3^{2-}$

Optimized structure without molecules of solvent in presented in Fig. 24. Two CO_3^{2-} ligands are distorted out off equatorial plane and their coordination mode towards uranium is monodentate. Explicit inclusion of solvent molecules allow carbonate ligands to stay in the coordination plane, Fig. 25 shows two possibilities differing by 486 cm^{-1} (the left one has been found as lower by energy and is presented first in Tab. 15).

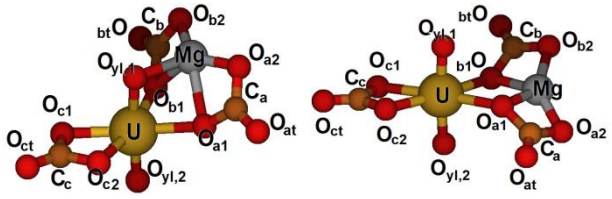

Fig. 24. Optimized structures (def-TZVPP basis) for $MgUO_2(CO_3)_3^{2-}$ in vacuum.

Inclusion of 22 water molecules to model led Mg atom to stabilize closer to equatorial, ligation, plane (Fig. 26-28). Bond lengths are given in Tab. 24 (for description, please see Fig. 24 and Fig. 25)

Table 15: Ground electronic state properties of $MgUO_2(CO_3)_3^{2-}$ (U-O_{yl} bond length R in pm, vibrational frequency of modes containing significant part of UO_2^{2+} symmetric stretching mode $\omega_{gs,1}$ and $\omega_{gs,2}$ [cm^{-1}]) and vertical excitation energies T_e [cm^{-1}].

ref	b.	*n*	*E*	T_e	$\omega_{gs,1}$	$\omega_{gs,2}$	*R*
1	S	0	0	19345	778	717	183
2	S	0	757	19845	841	729	180
4	T	0	-1194	19210	769	707	183
5	T	0	-1193	19697	840		179
7	S	12	0	20837	*850*	*700*	183
8	S	12	638	20647	825		180
9	S	12	710	20737	802		181
10	Tc	12	0	20470	*850*	*765*	184
11	Tc	12	486		823		180
12	Tc	12	1326		801		180
13	S	22	0	21209	824		181
14	S	22	127	21403	831		180
15	Tc	22	0	**21315**	**820**		180
16	Tc	22	625	21206	826		178

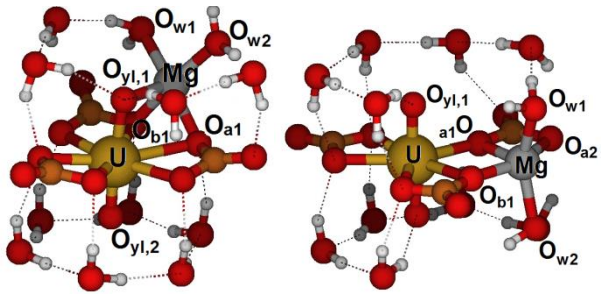

Fig. 25. Optimized structures (def-TZVPPc basis) for $MgUO_2(CO_3)_3^{2-} \cdot 12H_2O$.

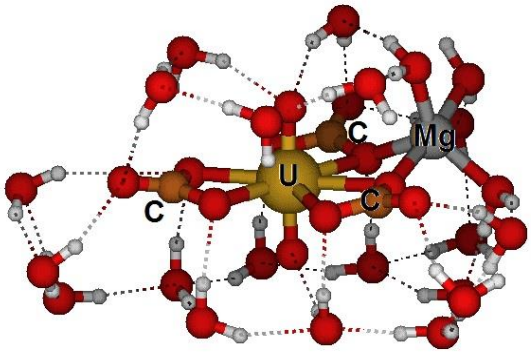

Fig. 26. Optimized structure (def-TZVPPc) for $MgUO_2(CO_3)_3^{2-} \cdot 22H_2O$. „Side view". All carbonate ligands are bidentate coordinated and Mg atom is only slightly above coordination plane, its coordination number is 5.

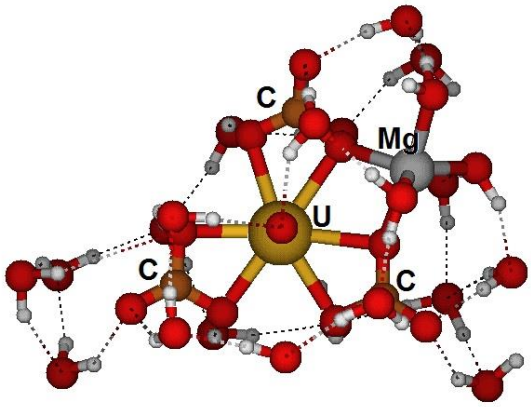

Fig. 27. Optimized structure (def-TZVPPc) for $MgUO_2(CO_3)_3^{2-} \cdot 22H_2O$. „Top view"

Table 16. Lengths of important bonds in $MgUO_2(CO_3)_3^{2-} \cdot n$ H_2O model structures.

ref	$MgO_{yl,l}$	MgO_{a1}	MgO_{a2}	UO_{a1}	UO_{a2}	UO_{c1}
4	212	224	193	231	231	228
5		203	194	241	241	229
10	212	202	**MgO_{b1}**	260	245	234
11		231	**198**	231		236
15		205	**200**	249	249	241
16		200		239	252	240

For ref. 14 (Tab. 15) also T_{de} = 20070 cm^{-1}, ΔR = 4.1 pm and T_a = 20758 cm^{-1} ($\Delta T = T_e - T_a$ = 645 cm^{-1}) has been calculated from excited state geomtery optimization.

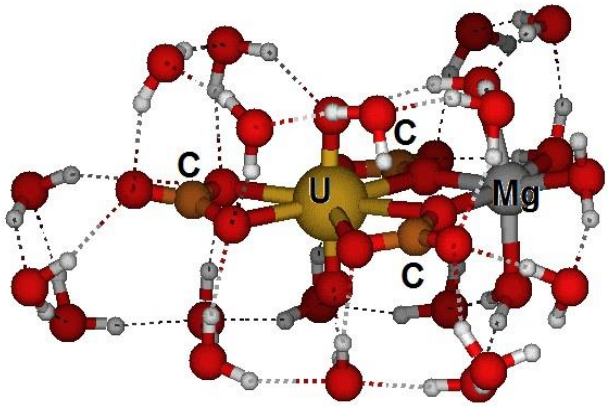

Fig. 28. PES local minimum structure (def-TZVPPc) for $MgUO_2(CO_3)_3^{2-} \cdot 22H_2O$. „Side view". All carbonate ligands are bidentate coordinated and Mg atom position is in coordination plane, with coordination number 6. This structure is 625 cm^{-1} higher than the one from Fig. 27.

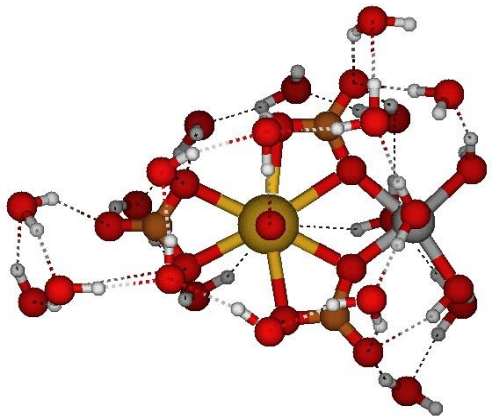

Fig. 29. „Down view" on structure from Fig. 28.

6.5 Ternary complex $CaUO_2(CO_3)_3^{2-}$

Detailed parametric study on number of explicit water included will be given in Supplementary Information. For highest number of explicit water molecules Ca atom prefered position slightly above coordination plane (Fig. 30-32) and tendency to coordination number 7 (Fig. 32).

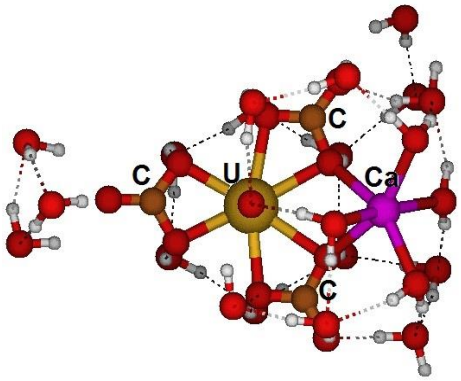

Fig. 30. Top view on optimized $CaUO_2(CO_3)_3^{2-} \cdot 22H_2O$ structure (within def-SVP atomic basis set), associated with ω_{gs} = 797 cm^{-1}, R = 181 pm and T_e = 21256 cm^{-1}.

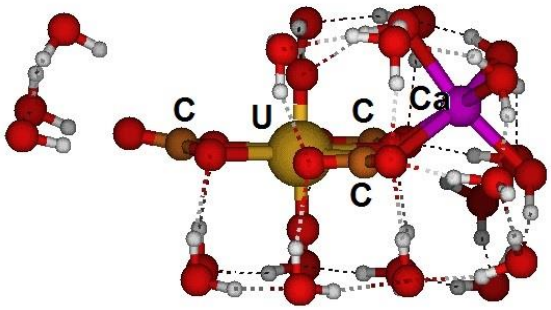

Fig. 31. Side view on optimized $CaUO_2(CO_3)_3^{2-} \cdot 22H_2O$ structure (within def-SVP atomic basis set, see Fig. 30)

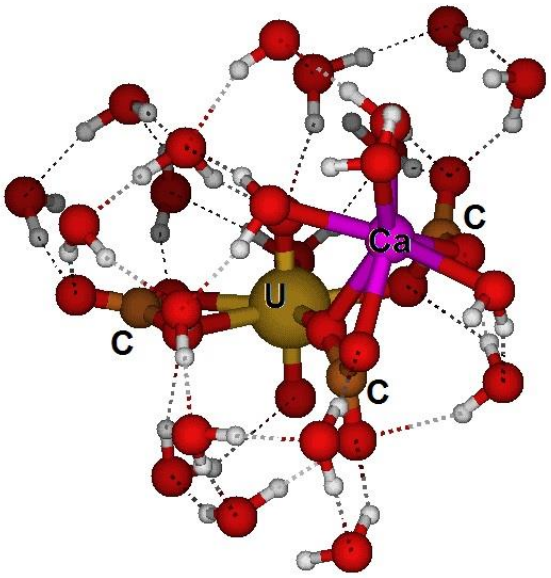

Fig. 32. optimized $CaUO_2(CO_3)_3^{2-} \cdot 22H_2O$ structure (within def-TZVPPc atomic basis set, see Tab. 17)

Spectroscopic properties are listed in Table 15 below.

Table 15: Calculated properties of $CaUO_2(CO_3)_3^{2-} . 22H_2O$

	b.	E	T_e	$\omega_{gs,1}$	$\omega_{gs,2}$	R
1	S		21256	797		181
2	Tc	0	**20401**	**811**	**794**	181
3	Tc	1837cm^{-1}	20475	824		180
4	Tc	2559cm^{-1}	21184	810		181

6.6 Ternary complex $Ca_2UO_2(CO_3)_3^0$

Similar features as in charged complex $CaUO_2(CO_3)_3^{2-}$ has been found for neutral bicalcium analogue $Ca_2UO_2(CO_3)_3^0$ as well (Fig. 33, 34, table 16)

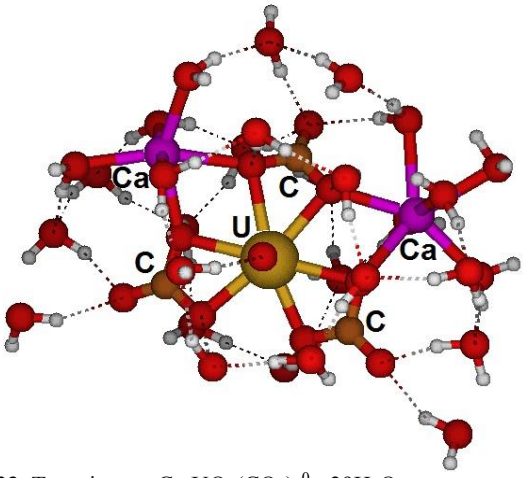

Fig. 33. Top view on $Ca_2UO_2(CO_3)_3^0 \cdot 29H_2O$ structure (optimized within def-SVP atomic basis set)

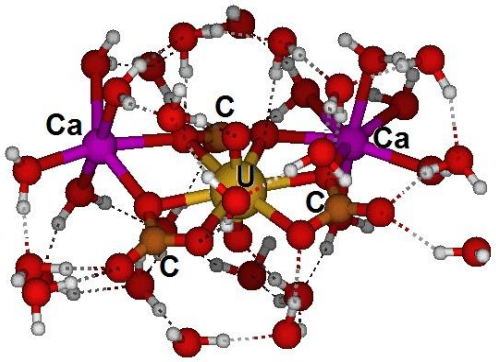

Fig. 34. $Ca_2UO_2(CO_3)_3^0 \cdot 29H_2O$ structure (optimized within def-SVP atomic basis set)

Table 16: Calculated properties of $Ca_2UO_2(CO_3)_3^0 . nH_2O$ models.

	b.	*n*	T_e	$\omega_{gs,1}$	$\omega_{gs,2}$	*R*
2	Tc	22		840		179
3	S	29	**21311**	**832**	**842**	180

6.7 On other molecular formation

Except for UO_2SO_4 (which has been studied in [1]) all uranyl complex species present in list of assigned species in Tab. 8 has been investigated by quasirelativistic (TD)DFT/B3LYP/D3 methodics here. However, the yet used geochemical models doesn't consider theoretically possible creation of

1) ternary alkaline metal-uranyl-carbonate species (e.g. $NaUO_2(CO_3)_3^{3-}$, ..., $Na_3UO_2(CO_3)_3^-$) [103]
2) ternary metal-uranyl-carbonate species with less than three carbonate ligands (e.g. $CaUO_2(CO_3)_2^0$, $NaUO_2(CO_3)^+$, ...)
3) uranyl complex species with two or more different ligands (e.g. $UO_2(HCO_3)(CO_3)_2^{3-}$)
4) quaternary metal-uranyl-carbonate species (e.g. $CaMgUO_2(CO_3)_2^0$) [102]

As a future prospect, thermodynamic constants determining stability/equilibrium concentrations of species ($\Delta G°$, $\Delta H°$, $\Delta S°$) should be calculated (for species listed in 1)-4) to decide on their importance and eventually to include them inside the geochemical speciation modelling as well)

6.8 Summary

In the following tables, parameters ω_{gs} (Tab. 17) and T_{00} (Tab. 18) estimated from

$$T_{00,m} \doteq T_{e,m} + \Delta T_{bc}, \quad (31)$$

(where $\Delta T_{bc} = T_{00,bc} - T_{e,bc} = 677$ cm^{-1} is an average of difference of adiabatic T_{00} and vertical T_e excitation energies computed for $UO_2(CO_3)_2^{2-}$ (807 cm^{-1}) and $T_a - T_e$ computed for $UO_2(CO_3)_3^{4-}$ (547 cm^{-1})) are compared to experimental values resulting from PARAFAC individual component assignment ("PF"), FATS results for samples S9 and S4 ($f = 4$) and to literature data.

Table 17: 0' → 0 transition energies T_{00} compared. QCH = from quasirelativistic TDDFT/B3LYP quantum chemical calculation presented here (bold underlines values of T_e in Tab. and relation (31)), PF = PARAFAC derived experimental value, FATS = FATS derived exp. value, Lit. = transition energy derived from linear fit of last three peak positions in HZDR report [66], with ref. being the corresponding literature source.

Species	QCH	PF	FATS	ref.	Lit.
$CaUO_2(CO_3)_3^{2-}$	19724	20051	19990	[66]	19948
$Ca_2UO_2(CO_3)_3$	20634	19916	19930	[73]	19943
$UO_2(CO_3)_3^{4-}$	20391	19858		[74]	20007
$MgUO_2(CO_3)_3^{2-}$	20638	19973	19970		
UO_2CO_3	20186	20089	20020	[67]	20081
UO_2SO_4 [s]	19729	19970	19920		
$UO_2(CO_3)_2^{2-}$	19830	19914			

Table 18: Symmetric stretching vibrational mode of uranyl group UO_2^{2+} in ground electronic state, sense of symbol is identical to that in previous Tab. 17.

Species	QCH	PF	FATS	ref.	Lit.
$CaUO_2(CO_3)_3^{2-}$	811 (794)	806	799	[66]	814
$Ca_2UO_2(CO_3)_3$	832 (842)	823	807	[73]	798
$UO_2(CO_3)_3^{4-}$	863	812[t]		[74]	792
$MgUO_2(CO_3)_3^{2-}$	820	797	806		
UO_2CO_3	852	817	827	[67]	815
UO_2SO_4	880[u]	831	819		
$UO_2(CO_3)_2^{2-}$	827	798			

[s] Calculated from Tab. 19 in [1] values of T_e and $\omega_{gs,1}$ corresponding to the first row for $[UO_2(\kappa^2\text{-}SO_4)(H_2O)_3] \cdot 10H_2O$.
[t] Ikeda et al [103] performed quasirelativistic quantum chemical calculation (DFT/B3LYP), but used different atomic basis set reporting 810.6 cm^{-1}, value very close to one from PARAFAC.
[u] From average from [1], for details, please see [76], [77].

Gray highlighted values in Tab. 17 and 18 have uncertain assignment to the corresponding two chemical species UO_2CO_3 / UO_2SO_4 (they could be swaped (but either in both tables simultaneously or not at all)).

7 Conclusions

Since the signal:noise ratio in measured natural water samples has been very low (yet very low differences between all spectroscopic parameters of individual components (in few to tens cm^{-1}) imply the decomposition into individual components is ill-conditioned problem and would demand signal:noise ratio to be rather high instead), for most samples, PARAFAC as a robust (exploiting correlations across wider set of data) chemometric method should be used. For eight component model (one component corresponds to artifact due to software background correction) individual component concentration profiles has been correlated to geochemical modelling prediction (done in [66] with EQ3/6 program [68], repoduced by us within PhreeqC [69] as well). Assignment of individual component spectra and luminescence decay curves is presented in Tab. 8. In following Tab. 9 literature data on spectroscopic parameters of assigned chemical components are listed. From comparison of identical parameters in aforementioned tables we can conclude that internal consistency of PARAFAC data analysis is relatively good (in particular for luminescence life-times τ and symmetric mode stretching frequency of uranyl group ω_{gs}).

Samples S4 and S5 are specific since they were produced by acidification of the sample S3 by HCl. In particular, sample S4 (pH = 5.5) should have qualitatively different speciation than other samples (Fig. 19, for S4 species UO_2CO_3 and UO_2SO_4 should be dominant over ternary tris(carbonato) complexes $M_nUO_2(CO_3)_3^{2n-4}$ (M = Ca,Mg, n = 0,1,2)). This might be overlooked by PARAFAC, but should be visible in detailed interpretation of FATS results for the samples S3, S4 and S5.

And FATS method truly indicate a one or two chemical components in S4 qualitatively different from the three seen as main constituents of all other samples – $Ca_2UO_2(CO_3)_3^0$, $CaUO_2(CO_3)_3^{2-}$ and $MgUO_2(CO_3)_3^{2-}$.

Quantum chemical modelling led to realistic values of vibrational frequencies of each species individually (few percent errors) and geometry of $Ca_2UO_2(CO_3)_3^0$ well comparable with literature [96,97]. And because the differences between ω_{gs} of different species are, in some cases, rather parts in percent (i.e. < 8 cm^{-1}) than the several percent error of their QM prediction, direct usage of here applied quanctum chemical methodics (quasirelativistic TDDFT geometry optimization of nanoscale water droplets with studied complex inside) would be too ambitious. Excited state properties (including T_e) haven't been predicted with certainity useful in practical individual component assignment. The reason might be that most uranyl compounds has highly multi-reference character of excited states (excited states are not dominated by a single electron configuration as the UO_2^{2+} ground state) and more advanced, ab initio, method should be used (rather than TD-DFT). Spin-orbit coupling should be also included for excitate state properties (going beyond quasirelativistic approximation). Further improvement planned will connect quantum chemical calculations to ambient temperature molecular dynamics to generate more realistic statistical ensambles of spectroscopic properties for each species / its simulated luminescence spectrum.

Even though rigorous chemometric methodic has been used, the data are not enough to provide more certain insight into uranium speciation of given samples. However, the methodology presented as a road to qualitative results is itself of great importance for future use.

We would like to thank the Department of Nuclear Chemistry for support and the Czech Student Grant Agency (grant no. SGS16/250/OHK4/3T/14) for material support. Special thanks are for experimental collaborators from HZDR (Helmholtz-Zentrum Dresden-Rossendorf). Useful help and hints came from Dr. Šebesta, Fibich and Sláma. I would like to thank TESNAT 2017 Organizing Committee for hospitality and the opportunity to present my work. Access to computing and storage facilities: National Grid Infrastructure MetaCentrum (www.metacentrum.cz/en/index.html) under program CESNET LM2015042 is greatly appreciated. This work was conducted using the resources of the iOpenShell Center for Computational Studies of Electronic Structure and Spectroscopy of Open-Shell and Electronically Excited Species (http://iopenshell.usc.edu) supported by the National Science Foundation through the CRIF:CRF program.

References

1. J. Višňák, L. Sobek, *EPJ Web of Conferences* **128**, 02002 (2016).
2. R. J. Lakowicz, *Principles of Fluorescence Spectroscopy*, (Third Edition, Springer), (2006).
3. J. Višňák, *Master Thesis*, FNSPE, Czech Technical University (2010) (In Czech).
4. C. Moulin, I. Laszak, V. Moulin, and C. Tondre: *Appl Spectrosc* **52** (1998) 528.
5. J. Višňák, *Bachelor project*, FNSPE, Czech Technical University in Prague (2008) (In Czech).
6. G. Meinrath, *Aquatic Chemistry of Uranium*, Review Focusing on Aspects of Environmental Chemistry, (Freiberg On-line Geoscience Vol.**1**), (1998).
7. J. Višňák, J. Bok, A. Vetešník, Annual report of the Department of Nuclear Chemistry 2008-2010, Prague. http://www.jaderna-chemie.cz/data/documents/vyrocni_zpravy/AR2008-2010.pdf (page 23).
8. B. Rasmus: *PARAFAC. Tutorial & applications.* Chemometrics Group, Food Technology, Royal Veterinary & Agricultural University. Rolighedsvej 30, III, DK-1958 Frederiksberg C, Denmark, http://www.models.kvl.dk/~rasmus/presentations/parafac_tutorial/paraf.htm.

9. R. A. Harshman, (1970). UCLA Working Papers in Phonetics, **16**, 84 pp. (University Microfilms, Ann Arbor, No. 10,085).
10. R. Harshman, M. Lundy, The PARAFAC model for three-way factor analysis and multidimensional scaling, In *Research methods for multimode data analysis*, chapter 5, pages 122-215. Praeger, New York (1984).
11. Ch. F. Beckmann, S. M. Smith : Tensorial Extensions of Independent Component Analysis for Multi-Subject FMRI Analysis. FMRIB (Oxford Centre for Functional Magnetic Resonance Imaging of the Brain) Technical Report TR04CB1, Department of Clinical Neurology, University of Oxford, John Radcliffe Hospital, Headley Way, Headington, Oxford, UK, http://www.fmrib.ox.ac.uk/analysis/techrep/tr04cb1/tr04cb1/tr04cb1.html.
12. R. Harshman, and M. Lundy, (1994). Comput Stat Data An, **18**:39-72.
13. Y. Yokoyama, M. Moriyasu, S. Ikeda, J. inorg, nucl. Chem., (1976), **38**, pp. 132%1333. Pergamon Press.
14. H. D. Burrows, S. J. Formosinho, M. G. Miguel, F. P. Coelho, J. Chem. Soc., Faraday Trans. ***1***, (1976),**72**, 163-171, 10.1039/F19767200163.
15. R. Matsushima, S. Sakuraba, J. Am. Chem. Soc., (1971), *93* (**26**), pp 7143–7145, DOI: 10.1021/ja00755a004.
16. H. D. Burrows, S. J. Formosinho. J. Chem. Educ, (1978), **55** (*2*) p 125., DOI 10.1021/ed055p125.
17. M. E. D. G. Azenha, H. D. Burrows, S. J. Formosinho, M G. M. Miguel, J. Chem. Soc., Faraday Trans. I, (1989), **85**(*8*), 2625-2634.
18. DIRAC, a relativistic ab initio electronic structure program, Release DIRAC16 (2016), written by H. J. Aa. Jensen, R. Bast, T. Saue, and L. Visscher, with contributions from V. Bakken, K. G. Dyall, S. Dubillard, U. Ekstroem, E. Eliav, T. Enevoldsen, E. Fasshauer, T. Fleig, O. Fossgaard, A. S. P. Gomes, T. Helgaker, J. Henriksson, M. Ilias, Ch. R. Jacob, S. Knecht, S. Komorovsky, O. Kullie, J. K. Laerdahl, C. V. Larsen, Y. S. Lee, H. S. Nataraj, M. K. Nayak, P. Norman, G. Olejniczak, J. Olsen, Y. C. Park, J. K. Pedersen, M. Pernpointner, R. Di Remigio, K. Ruud, P. Salek, B. Schimmelpfennig, J. Sikkema, A. J. Thorvaldsen, J. Thyssen, J. van Stralen, S. Villaume, O. Visser, T. Winther, and S. Yamamoto (see http://www.diracprogram.org).
19. L. H. Jones, Spectrochim Acta, (1958), **l0**, pp.395-403. Pergamon Press Ltd., London.
20. Bartecki A., On the Theory of Uranyl Compounds in Solutions, in Theory and Structure of Complex Compounds, *Proceedings of the Symposium held at Wroclaw*, s. 233-247, (1964).
21. Ch. Görller-Walrand, S. De Houwer, L. Fluyt, K. Binnemans, Phys. Chem. Chem. Phys., (2004), **6**, 3292-3298.
22. V. E. Jackson, R. Craciun, D. A. Dixon, K. A. Peterson, W. A. de Jong, J. Phys. Chem. A, **112**, 4095-4099, (2008).
23. J. Višňák, J. Kuba, A. Vetešník, J. Bok, V. Sladkov UO2(2+) - XO4(2-) - H2O TRLFS and spectrophotometric speciation study (X=S, Se) In *Lectures of colloquium on Radioanalytical methods*, **IAA 14**, Edited by Jiří Mizera, Ioannes Marcus Marci Spectroscopic Society - IMMSS, ISBN 978-80-905704-4-3 (2014).
24. Z. Wang, J. M. Zachara, W. Yantasee, P. Gassman, Ch. Liu, Environ. Sci. Technol., **38**, 5591-5597 (2004).
25. M. Gal, P.L. Goggin, J. Mink, Spectrochim. Acta **48A** (1992).
26. J. T. Bell, R. E. Biggers, J. Mol Spectrosc, **25**, 312 (1986).
27. https://www.hzdr.de/db/Cms?pOid=14407&pNid=334
28. Molecular Spectroscopy and Chemical Dynamics, lecture text, Spring Term 2013, University of Basel, Department of Chemistry, http://www.chemie.unibas.ch/~willitsch/vtv_files/normal_modes_S.pdf .
29. R. Steudtner, personal communication at HZDR, 2017.
30. C. Eckart, G. Young, (1936). **1** (3): 211–8. doi:10.1007/BF02288367.
31. M. R. Hestenes, (1958). J Soc Ind Appl Math. **6** (1): 51–90. JSTOR 2098862. MR 0092215. doi:10.1137/0106005.
32. G. H. Golub, W. Kahan, (1965). **2** (2): 205–224. JSTOR 2949777. MR 0183105. doi:10.1137/0702016.
33. D. Vopálka et al, Report to the final control day with respect to the contract between Radioactive Waste Repository Authority (RAWRA) and Czech Technical University (FNSPE) (Phase 4) (n. 4007016), Prague, July 2009 (Chapter 2.2 (author: A. Vetešník), Chapter 2.3 (J. Višňák), Chapter 3 (J. Šebera)) (In Czech).
34. T. W. Anderson, *An Introduction to Multivariate Statistical Analysis*, (Wiley, New York, 1958).
35. K.V. Mardia, J.T. Kent, J.M. Bibby (1979). *Multivariate Analysis*. Academic Press,. ISBN 0124712525. (M.A. level "likelihood" approach).
36. R. A. Johnson, D. W. Wichern, (2007). *Applied Multivariate Statistical Analysis* (Sixth ed.). Prentice Hall. ISBN 978-0-13-187715-3.
37. J. Pfanzagl, with the assistance of R. Hamböker (1994). *Parametric statistical theory*. Walter de Gruyter, Berlin, DE. pp. 207–208. ISBN 3-11-013863-8.
38. L. J. Savage, (1976). The Annals of Statistics. **4** (3): 441–500. JSTOR 2958221. doi:10.1214/aos/1176343456.
39. J. W. Pratt, (1976). The Annals of Statistics. **4** (3): 501–514. JSTOR 2958222. doi:10.1214/aos/1176343457.
40. A. Hald, (1999). Stat Sci. **14** (2): 214–222. JSTOR 2676741. doi:10.1214/ss/1009212248.
41. J. Aldrich, (1997). **12** (3): 162–176. MR 1617519. doi:10.1214/ss/1030037906.

42. M. Hazewinkel, ed. (2001), "Maximum-likelihood method", *Encyclopedia of Mathematics*, Springer, ISBN 978-1-55608-010-4.
43. O. Y. Rodionova, A. L. Pomerantsev, Russ Chem Rev **75** (4) 271-287 (2006).
44. E. H. Moore, (1920). B Am Math Soc. **26** (9): 394–395. doi:10.1090/S0002-9904-1920-03322-7.
45. A. Bjerhammar, (1951). "Application of calculus of matrices to method of least squares; with special references to geodetic calculations". Trans. Roy. Inst. Tech. Stockholm. **49**.
46. R. Penrose, (1955). "A generalized inverse for matrices". *Proceedings of the Cambridge Philosophical Society*. **51**: 406–413. doi:10.1017/S0305004100030401.
47. G. H. Golub, F. V.L. Charles (1996). *Matrix computations* (3rd ed.). Baltimore: Johns Hopkins. pp. 257–258. ISBN 0-8018-5414-8.
48. A. Ben-Israel, T. N.E. Greville (2003). *Generalized Inverses*. Springer-Verlag. ISBN 0-387-00293-6.
49. J. Bečvář: *Linear Algebra*, matfyzpress, Praha 2002, chap. „Pseudoinverzní homomorfismy a matice“, 414-431 (In Czech).
50. R. G. Brereton, *Applied Chemometrics for Scientists*, University of Bristol, Wiley, 2007, ISBN-13: 978-0-470-01686-2.
51. J. N. Miller, J. V. Miller, *Statistics and Chemometrics for Analytical Chemistry*, Pearson Edu. L., Sixth edition 2010, ISBN: 978-0-273-73042-2.
52. J. Franck, (1926). T Faraday Soc. **21**: 536–542. doi:10.1039/tf9262100536.
53. E. Condon, (1928). Phys Rev **32**: 858–872. doi:10.1103/PhysRev.32.858.
54. A. S. Coolidge, H. M. James, R. D. Present, (1936). J Chem Phys **4**: 193–211. doi:10.1063/1.1749818.
55. P. W. Atkins, R. S. Friedman (1999). *Molecular Quantum Mechanics*. Oxford: Oxford University Press. ISBN 0-19-855947-X (page 386).
56. J.-L. Chang, J. Mol. Spectrosc., **232**, 102-104, (2005).
57. R. Islampour, M. Dehestani, S. H. Lin, J. Mol. Spectrosc. **194**, 179–184 (1999).
58. P.-A. Malmqvist, N. Forsberg, Chem. Phys., **228**, 227–240, (1998).
59. F. Duschinsky, Acta Physicochim. USRR **7**, 551 (1937).
60. P. T. Ruhoff, *Ph.D. Thesis*, Odense University, 1995.
61. I. J. Ozkan, Mol. Spec. (1990), **139**, 147-162.
62. A. W. Adamson, (1976), Adv Chem, **150** (Chap. 12). 128-148. ISBN13: 9780841202818, 10.1021/ba-1976-0150.ch012.
63. http://www.theanalysisfactor.com/factor-analysis-how-many-factors/
64. http://ba-finance-2013.blogspot.no/2012/09/scree-plots-interpretation-and.html
65. LabSpec, http://www.horiba.com/scientific/products/raman-spectroscopy/software/
66. R. Steudtner, H. Neubert, V. Brendler, B. Drobot, *Report zum Analysenauftrag „Nachweis und die Charakterisierung von Uran-Spezies in wässrigen Umweltproben“*, 2014, Institut für Bergbau der TU Bergakademie Freiberg (in Absprache mit Wismut GmbH).
67. Z. Wang, J. M. Zachara, W. Yantasee, P. L. Gassman, C. X. Liu, A. G. Joly. (2004) Environmental Science & Technology **38**: 5591-5597.
68. T.J. Wolery (1992). EQ3/6, A software package for the geochemical modelling of aqueous systems. UCRL-MA-110662 Part I, Lawrence Livermore National Laboratory.
69. D.L. Parkhurst, C.A.J. Appelo, (2013), Description of input and examples for PHREEQC version 3--A computer program for speciation, batch- reaction, one-dimensional transport, and inverse geochemical calculations: U.S. Geological Survey Techniques and Methods, book 6, chap. A43, 497 p., available only at http://pubs.usgs.gov/tm/06/a43.
70. R. Guillaumont, T. Fanghänel, J. Fuger, I. Grenthe, V. Neck, D. A. Palmer, M.H. Rand, (2003) Update on the chemical thermodynamics of uranium, neptunium, plutonium, americium and technetium. Chemical Thermodynamics Vol. 5 (OECD Nuclear Energy Agency, ed.), Elsevier, Amsterdam.
71. Bernhard, G., Geipel, G., Reich, T., Brendler, V., Amayri, S., Nitsche, H. (2001) Radiochim. Acta **89**: 511-518.
72. W. Dong, S. Brooks, (2006) Environ. Sci. Technol. **40**: 4689-4695.
73. A.A.A. Osman, (2014) *Ph.D. thesis,* TU Dresden, 124pp.
74. C. Götz, G. Geipel, G. Bernhard, (2011) J. Radioanal. Nucl. Chem. **287**:961-969.
75. S. V. Lotnik, L.A. Khamidullina, V.P. Kazakov, (2003) Radiochemistry **45**:499-502.
76. J. Višňák, L. Sobek, Quasirelativistic Quantum Chemical calculations of Uranyl(VI)-Sulfates Spectroscopic properties, in *Department of Nuclear Chemistry Annual Report* 2015-2016.
77. J. Višňák, L. Sobek L. (2017), *MetaCentrum Annual. Report*, in publication.
78. TURBOMOLE V6.5 2013, a development of University of Karlsruhe and Forschungszentrum Karlsruhe GmbH, 1989-2007, TURBOMOLE GmbH, since 2007; available from http://www.turbomole.com.
79. X. Cao, M. Dolg, J. Molec. Struct., **673**, 203-209 (2004).
80. M. Dolg, in Proceedings, Second Edition, J. Grotendorst (Ed.), John von Neumann Institute for Computing, Julich, NIC Series, **3**, pp. 507-540 (2000).
81. K. Eichkorn, O. Treutler, H. Öhm, M. Häser and R. Ahlrichs; Chem. Phys. Letters **242**, 652 (1995).
82. A. Schäfer, H. Horn, R. Ahlrichs, J. Chem. Phys., **97**, 2571 (1992).
83. F. Weigend et al, Chem. Phys. Letters **294**, 143 (1998).

84. P. Hohenberg, W. Kohn, Phys. Rev. **136** (3B): B864–B871, (1964).
85. W. Kohn, L. J. Sham, Phys. Rev. **140** (4A): A1133-A1138 (1965).
86. A. Szabo, N. S. Ostlund, *Modern Quantum Chemistry: Introduction to Advanced Electronic Structure Theory*, McGraw-Hill Publishing Company, New York, (1989).
87. E. Runge, E. K. U. Gross, Phys. Rev. Lett. **52** (12): 997–1000 (1984).
88. M. Petersilka, U. J. Gossmann; E.K.U. Gross, Phys. Rev. Lett. **76** (8): 1212–1215 (1996).
89. C. Ullrich, *Time-Dependent Density-Functional Theory: Concepts and Applications* (Oxford Graduate Texts), Oxford University Press, (2012).
90. A. D. Becke, J. Chem. Phys. **98** (7): 5648–5652 (1993).
91. S. Grimme, J. Antony, S. Ehrlich, Krieg, *J. Chem. Phys*, **132**, 154104 (2010).
92. G.Schaftenaar and J.H. Noordik, *J. Comput.-Aided Mol. Design*, **14**, 123-134, (2000).
93. O. Treutler, R. Ahlrichs, J Chem Phys **102**: 346 (1995)
94. R. Ahlrichs, M. Baer, M. Haeser, H. Horn, C. Koelmel, Chem. Phys. Lett. 162: 165 (1989)
95. F. Weigend, F. Furche, R. Ahlrichs, J. Chem. Phys. **119**, 12753 (2003).
96. S. Tsushima, Y. Uchida, T. Reich, Chem Phys Lett **357** (2002) 73-77.
97. A. O. Tirler, T. S. Hofer, Dalton Trans., (2016), **45**, 4983, DOI: 10.1039/c5dt04718h.
98. A. Vetešník, J. Višňák, MyExpFit V4 program.
99. MATLAB and Statistics Toolbox Release 2012b, The MathWorks, Inc., Natick, Massachusetts, United States.
100. Wolfram Research, Inc., Mathematica, Version 10.4, Champaign, IL (2016).
101. V.A. Mozhayskiy and A.I. Krylov, ezSpectrum, http://iopenshell.usc.edu/downloads
102. S. Amayri et al. J Solid State Chem **178** (2005) 567–577.
103. A. Ikeda et al, Inorg. Chem. (2007), **46**, 4212−4219.